

CBPF-NF-019/91

**ELECTRONIC STRUCTURE AND ELECTRIC FIELD GRADIENTS  
OF CRYSTALLINE Sn(II) AND Sn(IV) COMPOUNDS**

by

**Joice TERRA and Diana GUENZBURGER**

Centro Brasileiro de Pesquisas Físicas - CBPF/CNPq  
Rua Dr. Xavier Sigaud, 150  
22290 - Rio de Janeiro, RJ - Brasil

**ABSTRACT**

The electronic structures of clusters representing crystalline compounds of Sn(II) and Sn(IV) were investigated, employing the first-principles Discrete Variational method and Local Density theory. Densities of states and related parameters were obtained and compared with experimental measurements and with results from band structure calculations. Effects of cluster size and of cluster truncated bonds are discussed. Electric field gradients at the Sn nucleus were calculated; results are analysed in terms of charge distribution and chemical bonding in the crystals.

**Key-words:** Tin compounds; Electronic structure; Electric field gradients.

## 1 INTRODUCTION

The theoretical investigation of the origin and magnitude of electric field gradients in solids requires the knowledge of their electronic structure, obtained with methods which are devoid of parameters. Two choices are available, band-structure methods, which make use of the translational symmetry of the crystal<sup>(1)</sup>, and cluster methods<sup>(2)</sup>. In these last, the solid is represented by a finite cluster of atoms and, although the accurate description of the long-range interactions will depend on the number of atoms included, is well suited when addressing hyperfine properties, which depend largely on the electronic charge distribution around one particular atomic probe.

We present the results of first-principles electronic structure calculations for clusters representing Sn (II) compounds (SnO(black), SnF<sub>2</sub>(β), SnS and SnSe) and Sn (IV) compounds (SnO<sub>2</sub> and SnF<sub>4</sub>). These compounds have been investigated experimentally by Mössbauer spectroscopy of <sup>119</sup>Sn<sup>(3)</sup>, and they have quadrupole splittings ΔEQ that cover a wide range of values<sup>(1)</sup> (from 0.45 to 2.20mm/s). Since ΔEQ is a product of a nuclear and an electronic term, the electric field gradient, we have calculated this last for all the compounds and obtained information on how it is related to their electronic structure.

The cluster method employed is adequate for the problem, mainly for two reasons. First, electric field gradients depend mostly on the very local environment around the Sn probe (as will become clear further on) and this is well described with the clusters chosen, which are all centered around a Sn nucleus, where the electric quadrupole interaction takes place. Another good reason for employing a real-space cluster approach is the complexity of the crystal structure of these solids, which makes band-structure calculations cumbersome or impossible to be undertaken without simplifications.

Although, as mentioned, a large number of Mössbauer data for <sup>119</sup>Sn is available in the literature, the data are limited by the fact that Sn does not have an intrinsic magnetic moment, which would cause a magnetic splitting of the Mössbauer lines. Due to this fact, the sign of ΔEQ has not been determined, for most Sn solids. Theoretically, Sn Mössbauer

hyperfine interactions have received considerably less attention than those of  $^{57}\text{Fe}$ . In the years of great Mössbauer spectroscopy development ('60s), theoretical models based on crystal field and ligand field theories were available for Fe, as for other transition elements; however, no corresponding theories existed for Sn. In more recent years, although much more sophisticated and precise theoretical methods exist, the complexity of the crystal structures of most Sn compounds has discouraged the theoreticians; consequently, only a few electronic structure calculations for Sn solids have been reported in the literature, and, to our knowledge, this is the first calculation of electric field gradients in Sn crystalline compounds.

Although we had a great interest in electric field gradients, these were by no means the only focus of our calculations. In fact, the six compounds considered include bonding between Sn and anions that may be considered to vary between ionic and covalent, since Sn has both oxidation states +2 and +4, and the anions cover a wide range of electronegativities; accordingly, their electronic structures and charge distributions may be thus considered interesting *per se*, to help understand how chemical bonds occur in Sn solids.

Finally, we mention that, in the list of solids studied, three compounds at least have known important applications. The Sn (IV) compound  $\text{SnO}_2$  is a large-gap semiconductor<sup>(4)</sup>, and has been widely used as radioactive source in Mössbauer experiments<sup>(3)</sup>; technologically, its importance derives from the fact that it may be used as a transparent electrode.  $\text{SnO}_2$  has also an important application as "inorganic exchanger" in Inorganic Analytical Chemistry. The Sn (II) compounds SnS and SnSe are also semiconductors. Recent technological applications of Sn and Pb chalcogenides include the construction of lasers and detectors in the infrared region<sup>(4)</sup>.

The self-consistent cluster calculations were performed employing the Discrete Variational method<sup>(5)</sup> and Local Density theory<sup>(6)</sup>, for clusters representing the solids. The convergence of the results obtained with cluster size was investigated by performing calculations, for each compound, for clusters with different number of atoms. The clusters were embedded in the charge density of many layers of external atoms; the potential thus generated was made consistent with the cluster potential.

In Section II we give some details of the theoretical method and in Section III we describe the solids and the clusters chosen to represent them. In Section IV we give results on charge distributions and densities of states, making comparisons with related experimental results and band structure calculations, when available. In Section V we show results for electric field gradients and in Section VI we summarize our conclusions.

## 2 THEORETICAL METHOD

Electronic structure calculations were performed with the Discrete Variational method (DVM)<sup>(5)</sup> in the framework of Local Density theory<sup>(6)</sup>, for clusters of varying sizes representing each compound. A summary of the main features of the DVM method as employed here is given in what follows, as well as particular details pertaining to the present calculations; more about the theory may be found in the references given.

The purpose of the Discrete Variational method is to solve the set of one-electron Kohn-Sham equations<sup>(7)</sup> of Local Density theory for the cluster (in Hartree atomic units):

$$h\psi_1(\vec{r}) = \left[ -1/2\nabla^2 + V_c(\vec{r}) + V_{xc}(\vec{r}) \right] \psi_1(\vec{r}) = \epsilon_1 \psi_1(\vec{r}) \quad (1)$$

where  $\psi_1(\vec{r})$  are cluster orbitals expanded as linear combinations of symmetrized numerical atomic orbitals  $\chi_\mu^a$  (LCAO):

$$\psi_1(\vec{r}) = \sum_{\mu} \chi_{\mu}^a(\vec{r}) C_{\mu}^1 \quad (2)$$

The Coulomb potential  $V_c(\vec{r})$  includes both the nuclear attraction of the electrons and electron-electron repulsion, and  $V_{xc}(\vec{r})$  is a functional of the electronic density  $\rho(\vec{r})$  expressed as

$$\rho(\vec{r}) = \sum_I n_I |\psi_I(\vec{r})|^2 \quad (3)$$

-4-

where  $n_1$  is the occupation of orbital  $\psi_1(\vec{r})$ . The potential  $V_{xc}(\vec{r})$  considered here was that derived by Hedin and Lundqvist<sup>(8)</sup>, which takes into account both exchange and correlation.

The hamiltonian and orbitals are defined numerically in a 3-dimensional grid of points. Application of the Discrete Variational method leads to the secular equations, to be solved self-consistently:

$$([H] - [E][S])[C] = 0 \quad (4)$$

where the matrix elements of the hamiltonian and overlap matrices ([H] and [S], respectively), calculated with the atomic basis functions, are summations over the numerical grid, with weights defined as the volume per point. This grid is chosen to be regular (and thus allowing a precise polynomial numerical integration)<sup>(9)</sup> inside a sphere of radius equal to  $2a_0$  around the central Sn atom, a region containing core orbitals which vary steeply with the distance from the nucleus; outside this sphere and around the other atoms, a pseudo-random diophantine point-generator is used to define the points. The total number of points for the self-consistent calculations was of the order of 5,000 for the Sn sphere and 10,000 - 14,000 for the rest of the cluster's space.

To facilitate the calculation of the electron-electron repulsion integral, a model potential is defined<sup>(10)</sup>, by substituting the exact cluster electronic charge density  $\rho(\vec{r})$  by a model charge density  $\rho_H(\vec{r})$  which is a superposition of spherical charge densities centered on each nucleus

$$\rho(\vec{r}) \approx \rho_H(\vec{r}) \approx \sum_{n\ell I} d_{n\ell}^I \rho_{n\ell}^I(\vec{r}) \quad (5)$$

The charge densities are not truncated (as in the muffin-tin scheme), being allowed to overlap. In Eq. (5),  $\rho_{n\ell}^I(\vec{r}) = \sum_q |R_{n\ell}^q(r_q)|^2 Y_0^0(\hat{r}_q)$ , the summation is over a previously defined set of atoms and the superscript I represents a particular set. The coefficients  $d_{n\ell}^I$  are obtained variationally

by a least-squares fit to the exact density  $\rho(\vec{r})$ , with the condition

$$\sum_{nl} d_{nl}^I \int \rho_{nl}^I(\vec{r}) dv = N \quad (6)$$

where  $N$  is the total number of electrons in the cluster. In all crystals, the Sn atoms are all equivalent. However, since we focus primarily on the central Sn atom, for each cluster this atom was considered a set by itself in Eq. (5), and thus its contribution to the model potential was allowed to be different from that of all other Sn atoms, all kept in the same set. In SnS, all S atoms are equivalent, and were thus kept in the same set; this is also the case for Se in SnSe and O in SnO and SnO<sub>2</sub>. There are two types of F atoms in SnF<sub>2</sub> and SnF<sub>4</sub>, as will be discussed in the next section; accordingly, they contributed differently to the model potential. This last is made self-consistent.

As mentioned before, several layers of external atoms were considered, on which were placed charge densities to simulate the external crystal<sup>(11)</sup>. These charge densities were obtained from atomic numerical local density calculations, and were truncated to take into account the Pauli exclusion principle. The potentials of the remaining external charges were considered with the use of the Ewald procedure<sup>(12)</sup>. Atomic basis functions in Eq. (2) were also obtained with atomic calculations. A potential well with a depth of -2.0 hartrees is added to all atoms, during the atomic self-consistent calculations, to assure the convergence of the negative ions and to slightly contract the Sn valence atomic functions, thus adapting them better to a description of the crystal. The basis functions used were 4s, 4p, 4d, 5s and 5p for the central Sn atom in all compounds and 5s and 5p for the other Sn atoms. For S, the variational orbitals were 3s and 3p and for Se, 4s and 4p. All core orbitals not included in the variational basis were kept "frozen" after the first iteration in the self-consistent procedure for the cluster, after having been orthogonalized to the valence basis functions. For O and F, all orbitals were kept in the variational space.

To start the self-consistent procedure, each atom was considered

neutral, and, accordingly, there was no charge on the cluster. After the first convergence was achieved, a Mulliken<sup>(13)</sup> population analysis was performed and charges determined on each type of atom (types defined in the sense of Eq. (5)). Since the central Sn atom is best described, its charge is used to determine the charge on the cluster for the next convergence. For example, if the charge found for the central Sn was +1 in  $[\text{SnO}_8\text{Sn}_{12}]$  (representing SnO), the Oxygens are assumed to have charge -1 and the charge on the cluster is +5. For the next set of iterations, the total number of electrons is adjusted to this charge; moreover, new basis orbitals are generated for the charges and configurations obtained for the atoms in the cluster, as well as new atomic charge densities for the external atoms, obtained from the same configurations. This procedure is repeated until the populations and charges on the cluster atoms are similar to those in the atoms generating the basis, as well as for the external atoms that simulate the rest of the crystal. This rather tedious and computer time-consuming scheme was designed to achieve three purposes: (a) to consider a total charge in the cluster consistent with atomic charges found with the calculations; (b) to reduce basis-truncation effects, by using basis orbitals consistent with the atomic configurations in the cluster; (c) to reduce spurious cluster-size effects in the simulation of the solid, by providing an embedding consistent with the cluster.

A partial local density of states  $D_{nl}^q$  may be defined for each orbital  $(n, \ell)$  in atom  $q$ , by broadening the discrete levels  $\epsilon_i$  by Lorentzians<sup>(14)</sup>

$$D_{nl}^q(E) = \sum_i P_{nl,i}^q \frac{\sigma/\pi}{(E-\epsilon_i)^2 + \sigma^2} \quad (7)$$

where the sum covers all cluster orbitals, for which  $P_{nl,i}^q$  is the population of orbital  $(nl)$  of atom  $q$ . Here the half-width  $\sigma$  was taken as 0.035eV. The total density of states is then:

$$D(E) = \sum_{qnl} D_{nl}^q(E) \quad (8)$$



### 3 DESCRIPTION OF THE CRYSTALS AND OF THE CLUSTERS

In Table I is given some information on the crystalline structure of the compounds studied<sup>(15)-(21)</sup>, as well as on the clusters chosen to represent them. The last column of this Table gives the local point symmetry around the central Sn atom, placed at the origin; it may be seen that the complex crystal structures displayed by these solids give rise to very low point symmetries for the clusters. This feature makes the calculations more cumbersome, and places limits on the sizes of the clusters selected.

The first compound in the Table is SnO, which is tetragonal in its most common variety (black SnO) and has two molecules per unit cell<sup>(15), (16)</sup>. All Sn and all O atoms are equivalent. In Figure (1) is represented a portion of this solid, as well as two of the clusters considered, the smallest and the largest. The structure of SnO is made of layers, and each Sn atom is at the vertex of a square pyramid whose base is formed by four oxygens. To form the three clusters selected to represent this compound, we added to the first cluster four oxygen atoms, and then four Sn atoms. SnF<sub>2</sub> crystallizes in three distinct phases,  $\alpha$ ,  $\beta$  and  $\gamma$ , with respectively monoclinic, orthorhombic and tetragonal structures. We chose  $\beta$ -SnF<sub>2</sub> since its value of  $\Delta EQ$  is large, and we were interested in a wide range of values for  $\Delta EQ$ . The local environment of a Sn atom and the smallest cluster considered are depicted in Fig. (2). The very distorted nature of the crystal<sup>(17)</sup> gives rise to the lowest point symmetry for all clusters ( $C_1$ ). All Sn atoms are equivalent and there are two types of F atoms. Each unit cell contains four molecules.

The last two isomorphous stannous compounds, SnS and SnSe, crystallize in a layered structure similar to that of black phosphorous, which may be viewed as a distorted NaCl or rocksalt structure<sup>(15), (18)</sup>. In Fig. (3) are depicted a portion of the crystal structure of black P, which the crystal structures of these compounds resemble. In this figure is also shown the largest cluster chosen to represent both SnS and SnSe. All Sn and all S (or Se) atoms are equivalent. SnS and SnSe form with GeS and GeSe a subset of isomorphous IV - VI semiconductors, which may be obtained also in amorphous phase. The unit cells contain four molecules.

Stannic oxide,  $\text{SnO}_2$ , crystallizes in a rutile-type structure, in which each Sn atom is surrounded by six Oxygen first neighbors, in a distorted octahedral coordination<sup>(18), (19)</sup>. In Fig. (4) are depicted a portion of the solid and the largest cluster chosen to represent it. The unit cell of this crystal contains two molecules; all Sn and all O atoms are equivalent.

Finally, both a portion of the  $\text{SnF}_4$  crystal and the largest cluster selected to represent it are shown in Fig. (5). The solid has a layered structure<sup>(15), (20)</sup>, in which each Sn atom is six-fold coordinated to F atoms of two types, four equational in the x-y plane ( $F_{\text{eq}}$  in Table I) and two axial in the z axis ( $F_{\text{ax}}$  in Table I). The distance  $\text{Sn}-F_{\text{ax}}$  is shorter than  $\text{Sn}-F_{\text{eq}}$ . The Sn and  $F_{\text{eq}}$  atoms form a layer, with the  $F_{\text{ax}}$  atoms forming layers by themselves, above and below.  $\text{SnF}_4$  crystallizes in the tetragonal structure, with two molecules per unit cell; all Sn atoms are equivalent and, as described, there are two types of F atoms.

#### IV ELECTRONIC STRUCTURE AND CHARGE DISTRIBUTION

For each compound investigated, we were interested in assessing the effect of cluster size in the calculated electronic and hyperfine properties. As an example, we may analyse the case of SnO. As given in Table I, three clusters of different sizes were considered. In Fig. (6) are shown the one-electron energy levels scheme for the three clusters. It may be seen from this figure that adding the four oxygen atoms on the topmost plane of the smaller cluster (Fig. (1)) has a large effect, causing the energy levels to be pushed down and the gap to widen; addition of the four outermost Sn atoms on the xy plane to form the third cluster has a much smaller effect. This trend was also observed when we analysed the charge distribution between the atoms: the difference between the first and second clusters is much more pronounced than between the second and third.

In filling the energy levels in Fig. (6) according to the "aufbau" principle, as is coherent with Local Density theory, the number of electrons considered for each cluster is determined by the charge calculated as

described in Section II. If the cluster is not stoichiometric, i.e., if the proportion of Sn and anion atoms is not the same as in the solid, there will be a small excess of electrons (when the number of Sn atoms surpasses the stoichiometric proportion) or a small depletion (when the number of anion atoms is in excess). For example, for  $[\text{SnO}_8\text{Sn}_{12}]$ , representing SnO, with charge +7.32, there will be an excess of 2.68 electrons in orbitals 16e (degenerate). However, we are trying to describe the infinite solid, and so in all cases after the final convergence is achieved we define the Fermi level as it would be in the stoichiometric case, that is, the last occupied level of the anion p valence band ( $15a_1$  for  $[\text{SnO}_8\text{Sn}_{12}]$ ). Since these "artificially occupied" or "artificially depleted" levels do not contribute to the hyperfine interactions at the central Sn atom, this constitutes no problem.

In Table II are displayed the Mulliken<sup>(13)</sup> charges and populations for the Sn compounds, obtained for the largest clusters. It may be observed that the central Sn atom ( $\text{Sn}_c$ ) and the other Sn atoms in the clusters have similar charges, which is an indication that our cluster description of the solids is reasonably accurate. The central Sn atom in all cases is better described, since all its bonding capacity is fulfilled; the peripheral Sn atoms ( $\text{Sn}_p$ ) have some of their bonds truncated. This may be the reason for the fact that the more external Sn atoms have systematically larger positive charges than  $\text{Sn}_c$ , since they are more similar to the free ions  $\text{Sn}^{2+}$  and  $\text{Sn}^{4+}$ . Also related to this feature is the smaller 5s - 5p hybridization, as compared to  $\text{Sn}_c$ , of the more external Sn atoms of the Sn (II) compounds, which have configurations more similar to the free ion  $5s^25p^0$ .

Charges on the central Sn atom for the stannous compounds are related closely to the electronegativities of the anions. In fact, the larger positive charges pertain to the Sn atom in SnO and  $\text{SnF}_2$ ; accordingly, the electronegativities of O and F have the large values 3.5 and 4.0, respectively. The electronegativities of S and Se are lower and very similar (2.5 and 2.4 respectively). Large positive Sn charges correspond to smaller 5s and 5p populations; in particular, in the four stannous compounds,  $\text{SnF}_2$  has a much smaller degree of 5s - 5p hybridization than the others.

-10-

For the two stannic compounds,  $\text{SnO}_2$  and  $\text{SnF}_4$ , the Mulliken analysis gives similar charges, indicating similar degrees of ionicity in the bonds. In  $\text{SnF}_4$ , the charge on  $F_{ax}$  is slightly less negative than on  $F_{eq}$ .

For all cases studied, the charges found on Sn are quite far from the formal charges +2 and +4.

A common characteristic of all Sn (II) compounds is the presence of a "lone pair" of electrons, which are accommodated in a void space in the crystal, where a bond with an anion is missing (see Figs. (1) - (3)). In a Molecular Orbital (or "cluster orbital") picture such as the present one, this "lone pair" on the central Sn atom is described mainly by one (or more) cluster orbitals with significantly higher  $\text{Sn}_c$  5s and 5p contributions. In Table III are given the compositions of the "lone pair" orbitals of all four stannous compounds. It may be seen that in  $\text{SnF}_2$  the "lone-pair" orbital has considerably more 5s character, relative to 5p, than in the other compounds; in this compound, this orbital has also a much higher total 5s + 5p character, signifying a stronger localization of the "lone-pair" on the Sn atom. In the other stannous compounds, the 5s and 5p populations have small contributions from many valence orbitals and the "lone-pair" is thus more delocalized.

In Fig. (7) are given total and partial Density of States (DOS) diagrams for SnO, obtained for the largest cluster ( $[\text{SnO}_8\text{Sn}_{12}]$ ). In these and other diagrams, the Sn 5s and 5p DOS were described as an average over  $\text{Sn}_c$  and  $\text{Sn}_p$ , independently of the actual  $\text{Sn}_c/\text{Sn}_p$  proportion in the cluster. From this diagram we may analyze the electronic structure of this compound. The narrow band at lower energies is the O(2s); there is a very small Sn(4d) participation in this band, but the 4d levels are almost entirely all located at about 3eV lower energies, forming a very narrow band, not shown in the figure. The valence band of SnO is dominated by O(2p) levels; however, there is a considerable mixture with Sn(5s) and, to a lesser extent, Sn(5p). This mixture evidences the covalent nature of the Sn - O bond. The conduction band unoccupied levels are predominantly Sn(5p).

In Fig. (8) we show the local DOS for Sn(5s) and Sn(5p) orbitals, discriminated for the central Sn atom ( $\text{Sn}_c$ ) and the peripheral  $\text{Sn}_p$ . In the actual crystal, all Sn atoms are equivalent; the inequivalence found for the

$\text{Sn}_c$  and  $\text{Sn}_p$  DOS is a result of representing the solid by a finite cluster of atoms. As mentioned earlier, results for the central Sn atom are more meaningful, since it is better described. In general, this cluster effect affects mostly the empty conduction band levels; for this reason, we shall not make a quantitative analysis of optical properties of the compounds. For  $\text{SnO}$ , however, the existence of an energy gap of roughly 2eV is clearly seen in Figs. (7) and (8), which could place this compound in the category of a semiconductor. Regrettably, we could not find any experimental reports in the literature on the optical or transport properties of  $\text{SnO}$ .

In Fig. (8) may be also seen the peak near the Fermi energy which describes mostly the Sn 5s - 5p hybridization at the central Sn atom. This corresponds to a "lone-pair" orbital ( $15a_1$ , given in Table III), and it may be observed that the areas are roughly in the same proportion as the relative 5s - 5p populations.

In Fig. (9) we present DOS diagrams for the largest cluster ( $[\text{SnF}_{11}\text{F}_4]$ ) representing  $\text{SnF}_2$ . The lowest energy band differs markedly from that of  $\text{SnO}$ , in that it shows a large mixture of Sn(4d) and F(2s) orbitals. This results in a widening of the band and, of course, in an enhanced DOS. We could not find any report of photoelectron spectroscopy measurements for this compound; it would be very interesting if such experiments were performed, to test our prediction. We must keep in mind, however, that energy eigenvalues of Local Density theory (see Eq. (1)) are only approximately comparable to ionization energies, since Koopmans' theorem does not hold, as it does in Hartree-Fock theory. For more precise results, a "transition state" calculation for each energy level has to be performed<sup>(21)</sup>.

The valence band of  $\text{SnF}_2$  is predominantly F(2p); some Sn(5s) mixture is present, but these orbitals contribute mostly at higher energies, near the Fermi level, whereas the F(2p) levels are concentrated at lower energies. This points to a small mixture between the Sn and F orbitals, and thus to a pronounced ionic nature of this compound. There are two types of F atoms in  $\text{SnF}_2$ ; one of them has a wider 2p band. The conduction band is constituted almost entirely of Sn(5p) levels. The separation between the Sn(5s) and Sn(5p) levels is consistent with the much smaller degree of

-12-

hybridization found by population analysis in this compound (Table II), as compared to the others. In Fig. (10) are shown DOS diagrams separately for  $\text{Sn}_c$  and  $\text{Sn}_p$ ; the separation of Sn(5s) and Sn(5p) levels is seen clearly. The peak near the Fermi energy corresponding to the "lone-pair" orbital on  $\text{Sn}_c$  is seen in Fig. (10), and it is predominantly Sn(5s). A gap of roughly 3.5 eV is found for  $\text{SnF}_2$ .

The DOS diagrams of the last two Sn(II) compounds SnS and SnSe, represented by the largest clusters ( $[\text{SnS}_7\text{Sn}_8]$  and  $[\text{SnSe}_7\text{Sn}_8]$ , respectively), are depicted in Figs. (11) to (14). These two compounds present similar electronic structures. The lowest energy bands in Fig. (11) (SnS) and Fig. (12) (SnSe) are constituted solely of S(3s) or Se(4s) levels, with practically no mixture with Sn(4d). The valence band in both cases presents a large mixture between S(3p) or Se(4p) and Sn orbitals and it is separated in two groups of levels, the first with predominantly mixture with Sn(5s) and the second, at higher energies, with Sn(5p). In Figs. (13) and (14) are given separately the Sn(5s) and Sn(5p) contributions for central and peripheral atoms. In these diagrams, we can see the peaks related to the "lone-pair" orbitals (Table III) near the Fermi energy. The empty conduction levels are predominately Sn(5p).

Since these two compounds show a marked degree of mixture between Sn and anion valence orbitals, they form pronouncedly covalent bonds. Photoemission spectra are available<sup>(4), (22)</sup> and are shown in Figs. (11) and (12) for comparison. It may be seen that the general features of the spectra are reproduced by the calculations, in particular the separation of the valence p band in two groups of levels, as described above. The nature of the experimental peaks may thus be understood. The high density of levels around the Fermi energy and our poor description of the empty conduction band does not allow any estimate of the gaps, except to say that they are small (<1eV in both cases). In fact, experimental measurements for these two typical semiconductors of type IV - VI are available giving gaps of ~ 1.1eV for SnS and ~ 0.9 for SnSe<sup>(4), (23), (24)</sup>.

The DOS diagrams of the two Sn(IV) compounds studied,  $\text{SnO}_2$  and  $\text{SnF}_4$ , are given in Figs. (15) to (18). These results are for the largest clusters

-13-

( $\{\text{SnO}_{10}\text{Sn}_{10}\}$  and  $\{\text{SnF}_{22}\text{Sn}_4\}$ ). The lowest energy band of  $\text{SnO}_2$  is predominantly O(2s); however, it does show a small Sn(4d) participation, as seen in Fig. (15). The valence band is almost entirely constituted of O(2p) levels, with very small admixture of Sn(5s) and (5p); in spite of its ionic nature,  $\text{SnO}_2$  is classified as a wide-gap semiconductor, with measured gap of  $3.6\text{eV}^{(4)}$ .

The DOS diagram of  $\text{SnF}_4$  depicted in Fig. (16) shows that the lower energy band has considerable Sn(4d) and F(2s) mixture. Again, it would be very interesting if photoemission spectra were obtained, to verify our predictions. Since there are two types of F atoms in the crystal, there are two F(2s) sub-bands. This fact, plus the mixture with Sn(4d), widens the F(2s) band. The valence band of  $\text{SnF}_4$  is formed almost entirely of F(2p); again, the two types of F contribute with two different sub-bands. The band constituted of the 2p levels of the equatorial F atoms is considerably wider; this may be understood by examining Fig. (5), where the structure of this solid is depicted. In fact, the equatorial F atoms are placed in layers in which each F is bonded to two Sn atoms; in contrast, the axial F atoms are more isolated and, accordingly, form a narrower 2p band.

The separated  $\text{Sn}_c$  and  $\text{Sn}_p$  5s and 5p local DOS are shown in Fig. (17) for  $\text{SnO}_2$  and Fig. (18) for  $\text{SnF}_4$ . For these two ionic compounds, the artificial difference between the central Sn and peripheral Sn atom bands is more pronounced than for the Sn (II) compounds. This fact may be understood by examining Figs. (4) and (5) where the clusters representing these solids are depicted. Due to the nature of the crystal structures, the more external Sn atoms in the clusters chosen are quite isolated.

As was described, for all compounds investigated, mixtures between the anion valence s orbitals and Sn(4d) were found for  $\text{SnF}_2$ ,  $\text{SnF}_4$  and, to a much lesser extent, for  $\text{SnO}_2$ . This mixture is very small in SnO and unexistent in SnS and SnSe. To understand better these differences, we performed Local Density self-consistent calculations for Sn, O,F,S and Se atoms. The valence s energy levels of F,O,S and Se are shown, together with the Sn(4d) level, in Fig. (19). In this figure, we observe that the F(2s) level is nearest in energy to the Sn(4d), followed by O(2s), whereas the S(3s) and Se(4s) levels are at much higher energies.

In Table IV we have collected some parameters related to the energy levels distributions in the Sn compounds. For comparison, we have included in this Table some experimental data found in the literature<sup>(22), (25)</sup>, as well as results from reported band structure calculations<sup>(26)-(30)</sup>.

The anion s valence band is narrow in all cases, being somewhat wider for SnF<sub>2</sub> and SnF<sub>4</sub> due to the existence of two different types of F atoms in both cases, as well as mixture with Sn(4d). The calculated values of this width  $\Delta_v^s$  for SnS and SnSe are smaller than those reported in the literature derived from photoemission spectra<sup>(22)</sup>; however, at least part of this discrepancy may be ascribed to the strong dependency of the resolution of the experimental peak on the photon energy. Band structure calculations with a parametrized Tight-Binding method<sup>(26)</sup> also give smaller values for  $\Delta_v^s$ , in agreement with ours.

The values of the width  $\Delta_v^p$  of the anion p valence band are similar in all compounds; the larger values of  $\Delta_v^p$  pertain to SnF<sub>2</sub> and SnF<sub>4</sub>, in which there are two types of F atoms, broadening this band. The calculated values of  $\Delta_v^p$  may be compared to values taken from photoelectron spectroscopy for SnS<sup>(22)</sup>, SnSe<sup>(22)</sup> and SnO<sub>2</sub><sup>(25)</sup>; these last are somewhat wider.

We only found reported band structure calculations for the semiconductors SnS, SnSe and SnO<sub>2</sub>. Parke and Srivastava<sup>(31)</sup> employed a semi-empirical pseudopotential method to study SnS; Car et al.<sup>(32)</sup> investigated SnSe with a similar method. Robertson<sup>(26)</sup> employed a Tight-Binding parametrized method to calculate the band structure of SnS and SnSe and obtained DOS diagrams similar to ours, although he assumed the FCC structure for these compounds.

Arlinghaus performed band structure calculations for SnO<sub>2</sub> employing the APW method<sup>(27)</sup>, with the "muffin tin" approximation for the potential in the solid. This calculation was the only one found by us in which the Sn(4d) orbital was considered. Jacquemin and Bordure<sup>(33)</sup> employed the KKR (Green's Function) method to SnO<sub>2</sub>, also within the "muffin tin" approximation. Robertson<sup>(28)</sup> also studied this compound with a parametrized Tight-Binding method; finally, Svane and Antoncik<sup>(29)</sup> studied SnO<sub>2</sub> with the LMTO (Linear Muffin-Tin Orbitals) method in a scalar-relativistic approach.



Another LMT0 calculation<sup>(30)</sup> for  $\text{SnO}_2$  gave a quite different result for the valence band width.

In Table IV we collect results for  $\Delta_v^P$  obtained with band calculations. We may observe that the Tight-Binding method gives values of  $\Delta_v^P$  which are larger than those obtained by us. For  $\text{SnO}_2$ , the APW and LMT0 methods give smaller values of  $\Delta_v^P$  than the Tight-Binding method; the value obtained by Svane and Antoncik with the LMT0 method for this parameter coincides with that obtained with the present calculation.

The values of  $\Delta_v^P$  for  $\text{SnO}_2$  obtained with the different band-structure calculations differ among themselves quite noticeably. The experimental value from photoemission spectroscopy indicates the larger value of  $\Delta_v^P$  as more correct; however, as pointed out by Svane and Antoncik, one must have caution when considering band widths derived from these photoemission experiments, due to certain experimental difficulties.

## V ELECTRIC FIELD GRADIENTS

The electric field gradient traceless tensor of components  $V_{jl}$ , in the system of principal axis, in which it is diagonal, is completely defined by one of its components  $V_{zz}$  and the so-called assymetry parameter  $\eta$  defined as<sup>(3)</sup>:

$$\eta = \frac{V_{xx} - V_{yy}}{V_{zz}} \quad (9)$$

The components are labeled according to the convention

$$|V_{zz}| \geq |V_{yy}| \geq |V_{xx}| \quad (10)$$

This limits the values of  $\eta$  to the range  $0 \leq \eta \leq 1$ .

For the 23.8 keV transition of  $^{119}\text{Sn}$ , the Mössbauer quadrupole splitting is given by

$$\Delta EQ = \frac{e V_{zz} Q}{2} \left[ 1 + \frac{\eta^2}{3} \right]^{1/2} \quad (11)$$

where  $Q$  is the quadrupole moment of the nucleus in the excited state and  $e$  the charge of the electron.

The term "electric field gradient" is used when referring to the largest component  $V_{zz}$ . In our Local Density cluster calculations, the components of the electric field gradient tensor, prior to diagonalization, are given by (in atomic units):

$$V_{j\ell} = - \int \rho(\vec{r}) \left( 3x_j x_\ell - \delta_{j\ell} r^2 \right) / r^5 dv + \sum_q Z_q^{ef} \left( 3x_{qj} x_{q\ell} - \delta_{j\ell} r_q^2 \right) / r_q^5 + \sum_p K_p \left( 3x_{pj} x_{p\ell} - \delta_{j\ell} r_p^2 \right) / r_p^5 \quad (12)$$

In Eq. (12), the first term is the electronic contribution, with  $\rho(\vec{r})$  given by Eq. (3); the second term is the point charge contribution of the nuclei of the cluster atoms around the central Sn atom where the electric field gradient is calculated, with  $Z_q^{ef}$  the nuclear charge minus the frozen core electrons. The third term represents the point charge contribution of the shells of neighbors external to the cluster present in the embedding, with charges  $K_p$  defined by the Mulliken population analysis for the corresponding atoms in the cluster.

The tensor with components  $V_{j\ell}$  is diagonalized to obtain the principal components and their direction. The principal components are then renamed according to the convention expressed in Eq. (10), independently of the cluster coordinate system.

The diagonal components of the  $V$  tensor at the central Sn atom in the principal axis system were obtained for all the clusters representing each Sn compound, as given in Table I. Both the values of the principal components and the directions tend to become stable as the cluster size is increased,

indicating in all cases that the clusters are large enough to ensure reasonable convergence of this property with respect to the number of atoms. This result asserts that cluster calculations are an adequate tool to calculate electric quadrupole interactions in ionic and covalent solid Sn compounds, and is an indication of the short-range nature of such interactions. Cautious systematic investigations of cluster size effects such as the present ones are, however, necessary, since results for small clusters may be completely misleading. For example, calculations for the smaller cluster representing SnS,  $[\text{SnS}_7\text{Sn}_2]$ , gave a value for  $V_{zz}$  which has the wrong sign and direction, when compared to the larger clusters  $[\text{SnS}_7\text{Sn}_6]$  and  $[\text{SnS}_7\text{Sn}_8]$ . The cluster  $[\text{SnO}_6]$  representing  $\text{SnO}_2$  gives a value of  $V_{zz}$  with opposite sign to those found for the larger clusters  $[\text{SnO}_6\text{Sn}_2]$  and  $[\text{SnO}_{10}\text{Sn}_{10}]$ , for which similar values of  $V_{zz}$  were obtained. This shows the importance of the contribution of the two Sn atoms in the z axis, above and below the xy plane, which were added to  $[\text{SnO}_6]$  to form the second cluster  $[\text{SnO}_6\text{Sn}_2]$  (see Fig. (4)).

In Table V are given the principal components and corresponding directions of the electric field gradient tensor at  $\text{Sn}_c$  for the largest clusters representing each compound. SnO and  $\text{SnF}_4$  have fourfold axial symmetry around the Sn atom; accordingly,  $V_{xx}$  and  $V_{yy}$  are degenerate on the xy plane. The negligibly small difference found between  $V_{xx}$  and  $V_{yy}$  for  $\text{SnF}_4$  is due to numerical errors. It is seen in this Table that values of  $V_{zz}$  are large and negative for all compounds except  $\text{SnO}_2$ , which has a small positive  $V_{zz}$  in the x direction (see Fig. (4)). SnO,  $\text{SnO}_2$  and  $\text{SnF}_4$  have axial symmetry around Sn, and so non-diagonal components of  $V_{ij}$  are zero and the cluster and principal coordinate systems coincide.

It was verified in all cases that the contribution of the shielded nuclei to  $V_{zz}$  (second term of Eq. (12)) and external charges contribution (third term of Eq. (12)) are very small; this shows that  $V_{zz}$  in these compounds are mainly determined by distortions of the electronic charge around the Sn atom, the effect of distant charges being much less important.

In Table VI we analyse the electronic contributions (first term in Eq. (12)) to the largest diagonal component of the tensor  $V_{ij}$ , prior to

-18-

diagonalization, i.e., in the cluster coordinate system. For the compounds with axial symmetry around Sn ( $\text{SnO}$ ,  $\text{SnO}_2$  and  $\text{SnF}_4$ ), these coincide with the electronic  $V_{zz}$ , since the axial symmetry determines that off-diagonal components be zero. This analysis may be performed by considering individual cluster orbitals in the definition of  $\rho(\vec{r})$  (Eq. (3)). In the first column of Table VI are given the shallow core contributions (cluster orbitals containing  $\text{Sn}_c(4s)$ ,  $(4p)$  and  $(4d)$ ); it may be verified that they are small compared to the total. The valence contribution has been decomposed in contributions from cluster orbitals containing  $5p_x$ ,  $5p_y$  and  $5p_z$  orbitals on the central Sn atom, in the LCAO basis; this decomposition is possible due to the symmetry properties of the cluster orbitals.

In  $\text{SnO}$  and  $\text{SnF}_4$ , the contribution of the orbitals containing  $5p_z$  dominates, and so they determine the sign and direction of  $V_{zz}$ . On the other hand, in  $\text{SnO}_2$  the largest (negative) contribution to  $V_{zz}$  comes from the orbitals containing  $5p_x$ ; however, the cluster orbitals containing  $5p_y$  and  $5p_z$  give positive contributions which, added together, surpass the  $5p_x$ , and so determine the positive sign of  $V_{zz}$ , which is on the x axis. For  $\text{SnS}$  and  $\text{SnSe}$ , the direction of  $V_{zz}$  is on the xy plane, and contributions of the orbitals containing  $5p_x$  and  $5p_y$  are dominant. No such analysis was possible for  $\text{SnF}_2$  due to the very low point symmetry.

In the last columns of Table VI are given the contributions of the "lone pair" cluster orbitals (see Table III), for the Sn(II) compounds. As seen in Table III, these orbitals contain  $\text{Sn}_c(5p_z)$  in  $\text{SnO}$  and  $\text{Sn}_c(5p_x + 5p_y)$  in  $\text{SnS}$  and  $\text{SnSe}$ . It may be verified that these orbitals are crucial in determining both the sign and direction of the electric field gradients.

In order to establish the validity of the frozen deep core approximation in the calculation of  $V_{zz}$ , we performed one test calculation for  $[\text{SnS}_7\text{S}_8]$  representing  $\text{SnS}$ , in which all orbitals on the central Sn orbital were included in the variational space. It was verified that the deep core ( $\text{Sn}(1s, 2s, 2p, 3s, 3p, 3d)$ ) contribution to  $V_{zz}$  was negligible, evidencing the almost spherical distribution of these electrons.

Finally, in Table VII are displayed the values of  $\Delta\text{EQ}$ , calculated according to Eq. (11), and compared to the experimental values measured by

Mössbauer spectroscopy<sup>(3), (34)-(36)</sup>. The value of the nuclear quadrupole moment adopted here was that derived by Haas et al.<sup>(37)</sup> ( $Q = -0.109b$ ).

We may verify from Table VII that the agreement between theoretical and experimental values of  $\Delta EQ$  is quite good for  $\text{SnF}_2$ ,  $\text{SnO}_2$  and  $\text{SnF}_4$ . For the other compounds the discrepancy is larger; however, results may be considered still fairly good, given the complexity of the crystals and of the property investigated. Since the agreement is best for the most ionic compounds, we believe the discrepancy found for  $\text{SnO}$ ,  $\text{SnS}$  and  $\text{SnSe}$  (which have more covalent, and thus more directional, bonds) most probably stems from the overlapping spherical approximation for the model density (Eq. (5)), since this would be worse for the more covalent bonds. The DV method allows for higher multipolar expansions of the model  $\rho_M^{(10)}$ ; however, more freedom for  $\rho_M$  in a cluster calculation may enhance the cluster-size effects. It must be mentioned also that some uncertainty should be allowed in the experimentally-derived value of  $Q$  adopted here.

For all compounds calculated,  $\Delta EQ$  is positive, except for  $\text{SnO}_2$ . Unfortunately, in the experiments reported the sign of this quantity was not measured for any compound; it would be very desirable if such measurements were performed, to test our predictions.

The Mössbauer Isomer Shifts of these Sn compounds were also investigated with the present calculations; results will be reported elsewhere<sup>(38)</sup>.

Preliminary results for electric field gradient calculations of these Sn compounds, using a somewhat different model potential, have been published elsewhere<sup>(39)</sup>.

## VI CONCLUSIONS

The electronic structure cluster calculations for Sn ionic and covalent compounds with complex crystal structures gave valuable insight into their electronic properties.

The charge distributions and DOS diagrams show that, of the Sn(II) compounds investigated,  $\text{SnF}_2$  is more ionic than  $\text{SnO}$ ,  $\text{SnS}$  and  $\text{SnSe}$ . For these

-20-

last three, considerable mixture between Sn and anion valence orbitals occur. The Sn(4d) orbitals combine with F(2s) to form a dense band at lower energies in SnF<sub>2</sub> and SnF<sub>4</sub>. This prediction could be tested if photoemission measurements were performed in this energy region.

Calculations of electric field gradients give interesting information on the origin of this quantity. Contributions of the charges outside the clusters are seen to be quite small, evidencing the local nature of Mössbauer quadrupole splittings. The importance of the "lone pair" electrons for the field gradients in Sn(II) compounds was assessed. Quantitative agreement with experimental values of  $\Delta EQ$  is very good for SnF<sub>2</sub>, SnO<sub>2</sub> and SnF<sub>4</sub>. Predictions for the signs of  $\Delta EQ$  in all compounds were made, calling for experimental verification.

#### ACKNOWLEDGEMENTS

The authors are indebted to D.E. Ellis for his interest and valuable discussions.

## TABLE CAPTIONS

Table I

Structural information on Sn(II) and Sn(IV) solids, clusters for which calculations were performed and symmetry group around central Sn atom. (a) See ref. (15). (b) See ref. (16). (c) From ref. (17). (d) From ref. (18). (e) From ref. (19). (f) From ref. (20).  $F_{eq}$  and  $F_{ax}$  stand for equatorial and axial F atoms, respectively (see Fig. (5)).

Table II

Charges and Mulliken populations in clusters representing Sn compounds.  $Sn_c$  is central Sn atom,  $Sn_p$  is peripheral Sn atom. F1 and F2 are the two types of F atoms in  $SnF_2$ ,  $F_{eq}$  and  $F_{ax}$  are equatorial and axial F atoms in  $SnF_4$ .

Table III

Population analysis of "lone pair" cluster orbitals of Sn(II) compounds.

Table IV

Energy distribution parameters (in eV) of Sn(II) and Sn(IV) compounds, for the largest clusters.  $E_f$  = Fermi energy,  $\Delta_v^s$  is width of valence s band,  $\Delta_v^p$  is width of valence p band. (a) From ref. (22). (b) From ref. (25). (c) From ref. (26). (d) From ref. (27). (e) From ref. (28). (f) From ref. (29). (g) From ref. (30). TB = Tight Binding, APW = Augmented Plane Wave, LMTO = Linear Muffin Tin Orbitals.

Table V

Principal components of the electric field gradient tensor around the central Sn atom and its directions in the coordinate systems of the clusters (see Figs. (1)-(5)).

Table VI

Analysis of the electronic contribution to the largest diagonal component

of the electric field gradient tensor prior to diagonalization. For clusters with axial symmetry ( $\text{SnO}$ ,  $\text{SnO}_2$  and  $\text{SnF}_4$ ), this coincides exactly with the electronic  $V_{zz}$ . For largest clusters.

### Table VII

Electric field gradient  $V_{zz}$  around Sn, assymetry parameter  $\eta$  and quadrupole splittings  $\Delta EQ$  of  $^{119}\text{Sn}$ . (a) From ref. (3). (b) From ref. (34). (c) From ref. (35). (d) From ref. (36).

### FIGURE CAPTIONS

#### Figure 1

a) Representation of portion of  $\text{SnO}$ (black) crystal, and of unit containing a Sn atom with "lone pair" electrons and four Oxygen nearest neighbors.

b) Smallest and largest clusters chosen to represent  $\text{SnO}$ .

#### Figure 2

a) Closest F neighbors environment surrounding Sn atom in  $\text{SnF}_2(\beta)$ . Dots represent "lone pair" electrons. F1 and F2 are the two types of F atoms in  $\text{SnF}_2$  crystal. Sn-nearest neighbor distances are also given (in Å).

b) Smallest cluster selected to represent  $\text{SnF}_2$ . The largest cluster is not shown due to the complexity of the low-symmetry structure.

#### Figure 3

a) Representation of the layered structure of black Phosphorous, to which the structures of  $\text{SnS}$  and  $\text{SnSe}$  are similar.

b) Largest cluster selected to represent isomorphous  $\text{SnS}$  and  $\text{SnSe}$ .

#### Figure 4

a) Unit cell and representation of portion of  $\text{SnO}_2$  crystal.

b) Largest cluster considered to represent  $\text{SnO}_2$ .



Figure 5

- View of portion of layered  $\text{SnF}_4$  crystal.
- Top view of same.
- Largest cluster selected to represent  $\text{SnF}_4$ .

Figure 6

One-electron energy levels of clusters representing  $\text{SnO}$ . Also shown are atomic levels of  $\text{Sn}$  and  $\text{O}$ , obtained with atomic Local Density calculations. Numbering of levels of smallest cluster  $[\text{SnO}_4\text{Sn}_8]$  is higher since, for this calculation, the 4s, 4p and 4d orbitals of peripheral  $\text{Sn}$  atoms were not frozen.

Figure 7

Total density of states (a) and partial densities of states of  $\text{SnO}$ , obtained for the cluster  $[\text{SnO}_8\text{Sn}_{12}]$ .

Figure 8

Partial DOS of central  $\text{Sn}$  ( $\text{Sn}_c$ ) and peripheral  $\text{Sn}$  ( $\text{Sn}_p$ ) atoms of the cluster  $[\text{SnO}_8\text{Sn}_{12}]$  representing  $\text{SnO}$ .

Figure 9

Total (a) and partial DOS of  $\text{SnF}_2$  obtained for the cluster  $[\text{SnF}_{11}\text{Sn}_4]$ . F1 and F2 are the two types of Fluorine atoms in the crystal.

Figure 10

Partial DOS of central  $\text{Sn}$  ( $\text{Sn}_c$ ) and peripheral  $\text{Sn}$  ( $\text{Sn}_p$ ) atoms of the cluster  $[\text{SnF}_{11}\text{Sn}_4]$ , representing  $\text{SnF}_2$ .

Figure 11

a) Photoelectron spectrum (from refs. (4) and (22)) of  $\text{SnS}$ . Total (b) and partial DOS of  $\text{SnS}$ , obtained for the cluster  $[\text{SnS}_7\text{Sn}_8]$ .

Figure 12

a) Photoelectron spectrum (from refs. (4) and (22)) of SnSe. Total (b) and partial DOS of SnSe, obtained for the cluster  $[\text{SnSe}_7\text{Sn}_8]$ .

Figure 13

Partial DOS of central Sn ( $\text{Sn}_c$ ) and peripheral Sn ( $\text{Sn}_p$ ) atoms of the cluster  $[\text{SnS}_7\text{Sn}_8]$ , representing SnS.

Figure 14

Partial DOS of central Sn ( $\text{Sn}_c$ ) and peripheral Sn ( $\text{Sn}_p$ ) atoms of the cluster  $[\text{SnSe}_7\text{Sn}_8]$ , representing SnSe.

Figure 15

Total (a) and partial DOS of  $\text{SnO}_2$ , obtained for the cluster  $[\text{SnO}_{10}\text{Sn}_{10}]$ .

Figure 16

Total (a) and partial DOS of  $\text{SnF}_4$ , obtained for the cluster  $[\text{SnF}_{22}\text{Sn}_4]$ .  $\text{F}_{\text{eq}}$  and  $\text{F}_{\text{ax}}$  are equatorial and axial Fluorine atoms, respectively.

Figure 17

Partial DOS of central Sn ( $\text{Sn}_c$ ) and peripheral Sn ( $\text{Sn}_p$ ) atoms of the cluster  $[\text{SnO}_{10}\text{Sn}_{10}]$ , representing  $\text{SnO}_2$ .

Figure 18

Partial DOS of central Sn ( $\text{Sn}_c$ ) and peripheral Sn ( $\text{Sn}_p$ ) atoms of the cluster  $[\text{SnF}_{22}\text{Sn}_4]$ , representing  $\text{SnF}_4$ .

Figure 19

Atomic energy levels of Sn, S, Se, O and F, obtained with atomic Local Density calculations.

TABLE I

Compound	Crystal Structure <sup>(a)</sup>	Lattice Parameters(Å)	Sn-X nearest-neighbor distances(Å)	Clusters	Local Symmetry
SnO(black) <sup>(b)</sup>	tetragonal	a = 3.80 c = 4.84	4(O) 2.22	[SnO <sub>4</sub> Sn <sub>8</sub> ] [SnO <sub>8</sub> Sn <sub>8</sub> ] [SnO <sub>8</sub> Sn <sub>12</sub> ]	C <sub>4v</sub>
SnF <sub>2</sub> (β) <sup>(c)</sup>	orthorhombic	a = 4.98 b = 5.14 c = 8.48	1(F) 1.89 1(F) 2.26 1(F) 2.40 1(F) 2.41 1(F) 2.49	[SnF <sub>5</sub> ] [SnF <sub>11</sub> Sn <sub>4</sub> ]	C <sub>1</sub>
SnS <sup>(d)</sup>	orthorhombic	a = 4.33 b = 11.18 c = 3.98	1(S) 2.62 2(S) 2.68 2(S) 3.27 1(S) 3.39	[SnS <sub>7</sub> Sn <sub>2</sub> ] [SnS <sub>7</sub> Sn <sub>6</sub> ] [SnS <sub>7</sub> Sn <sub>8</sub> ]	C <sub>s</sub>
SnSe <sup>(d)</sup>	orthorhombic	a = 4.46 b = 11.57 c = 4.19	1(Se) 2.77 2(Se) 2.82 2(Se) 3.35 1(Se) 3.47	[SnSe <sub>7</sub> Sn <sub>8</sub> ]	C <sub>s</sub>
SnO <sub>2</sub> <sup>(d)(e)</sup>	tetragonal	a = 4.74 c = 3.19	2(O) <sub>y</sub> 2.06 4(O) <sub>xz</sub> 2.05	[SnO <sub>6</sub> ] [SnO <sub>6</sub> Sn <sub>2</sub> ] [SnO <sub>10</sub> Sn <sub>10</sub> ]	D <sub>2h</sub>
SnF <sub>4</sub> <sup>(f)</sup>	tetragonal	a = 4.04 c = 7.93	4(F <sub>eq</sub> ) 2.02 2(F <sub>ax</sub> ) 1.88	[SnF <sub>6</sub> ] [SnF <sub>14</sub> Sn <sub>4</sub> ] [SnF <sub>22</sub> Sn <sub>4</sub> ]	D <sub>4h</sub>

TABLE II

Compound	SnO	SnF <sub>2</sub>	SnS	SnSe	SnO <sub>2</sub>	SnF <sub>4</sub>
Cluster	[SnO <sub>8</sub> Sn <sub>12</sub> ]	[SnF <sub>11</sub> Sn <sub>4</sub> ]	[SnS <sub>7</sub> Sn <sub>8</sub> ]	[SnSe <sub>7</sub> Sn <sub>8</sub> ]	[SnO <sub>10</sub> Sn <sub>10</sub> ]	[SnF <sub>22</sub> Sn <sub>4</sub> ]
Cluster charge	+7.32	-0.88	+2.72	+2.02	+19.69	-1.63
	$\left\{ \begin{array}{l} 4s \ 2.000 \\ 4p \ 6.000 \\ 4d \ 9.993 \\ 5s \ 1.365 \\ 5p \ 1.394 \\ +1.248 \end{array} \right.$	$\left\{ \begin{array}{l} 2.000 \\ 6.000 \\ 9.995 \\ 1.660 \\ 0.670 \\ +1.675 \end{array} \right.$	$\left\{ \begin{array}{l} 2.000 \\ 6.000 \\ 9.998 \\ 1.609 \\ 1.363 \\ +1.030 \end{array} \right.$	$\left\{ \begin{array}{l} 2.000 \\ 6.000 \\ 9.999 \\ 1.709 \\ 1.432 \\ +0.860 \end{array} \right.$	$\left\{ \begin{array}{l} 2.000 \\ 6.000 \\ 9.993 \\ 0.494 \\ 0.698 \\ +2.815 \end{array} \right.$	$\left\{ \begin{array}{l} 2.000 \\ 6.000 \\ 9.988 \\ 0.573 \\ 0.644 \\ +2.795 \end{array} \right.$
	$\left\{ \begin{array}{l} 2s \ 1.945 \\ 2p \ 5.303 \\ -1.248 \end{array} \right.$	$\left\{ \begin{array}{l} 2s \ 1.987 \\ 2p \ 5.875 \\ -0.862 \end{array} \right.$	$\left\{ \begin{array}{l} 3s \ 1.951 \\ 3p \ 5.126 \\ -1.077 \end{array} \right.$	$\left\{ \begin{array}{l} 4s \ 1.954 \\ 4p \ 4.896 \\ -0.850 \end{array} \right.$	$\left\{ \begin{array}{l} 2s \ 1.940 \\ 2p \ 5.448 \\ -1.388 \end{array} \right.$	$\left\{ \begin{array}{l} 2s \ 1.999 \\ 2p \ 5.760 \\ -0.759 \end{array} \right.$
	X	F1			F <sub>eq</sub>	F <sub>ax</sub>
	$\left\{ \begin{array}{l} 5s \ 1.568 \\ 5p \ 1.094 \\ +1.338 \end{array} \right.$	$\left\{ \begin{array}{l} 1.800 \\ 0.454 \\ +1.746 \end{array} \right.$	$\left\{ \begin{array}{l} 1.773 \\ 1.073 \\ +1.154 \end{array} \right.$	$\left\{ \begin{array}{l} 1.818 \\ 1.293 \\ +0.889 \end{array} \right.$	$\left\{ \begin{array}{l} 0.697 \\ 0.227 \\ +3.076 \end{array} \right.$	$\left\{ \begin{array}{l} 0.543 \\ 0.114 \\ +3.343 \end{array} \right.$

TABLE III

Compound	Cluster	Orbital	Energy (eV)	Population Analysis (in%)			
				Sn <sub>c</sub> (5s)	Sn <sub>c</sub> (5p)	Sn <sub>p</sub> Anion	
SnO	[SnO <sub>8</sub> Sn <sub>12</sub> ]	13a <sub>1</sub>	-12.22	8.6	8.5(5p <sub>z</sub> )	54.8	28.1
		15a <sub>1</sub>	-10.49	13.6	20.1(5p <sub>z</sub> )	36.3	30.0
SnF <sub>2</sub>	[SnF <sub>11</sub> Sn <sub>4</sub> ]	58a	-6.38	49.9	12.9	11.7	19.7(F1) 5.8(F2)
SnS	[SnS <sub>7</sub> Sn <sub>8</sub> ]	28a'	-9.35	12.8	14.9(5p <sub>x</sub> , 5p <sub>y</sub> )	18.5	53.8
SnSe	[SnSe <sub>7</sub> Sn <sub>8</sub> ]	28a'	-8.19	14.2	14.3(5p <sub>x</sub> , 5p <sub>y</sub> )	15.9	55.6

TABLE IV

	SnO	SnF <sub>2</sub>	SnS	SnSe	SnO <sub>2</sub>	SnF <sub>4</sub>
$E_f$	-10.4	-6.2	-9.2	-8.2	-17.5	-8.3
$\Delta_v^s$	2.1	3.9	-2.0	-2.0	2.3	3.0
$\Delta_v^p$	6.4	7.4	6.3	6.0	6.6	7.7
$\Delta_v^s$ (experimental)	-	-	-4 <sup>(a)</sup>	-5 <sup>(a)</sup>	-	-
$\Delta_v^p$ (experimental)	-	-	-10 <sup>(a)</sup>	-9 <sup>(a)</sup>	-9 <sup>(b)</sup>	-
$\Delta_v^s$ (band calculation)	-	-	-2.0(TB) <sup>(c)</sup> (FCC)	-2.0(TB) <sup>(c)</sup> (FCC)	-1.4(APW) <sup>(d)</sup> -2.0(TB) <sup>(e)</sup> -3.0(LMTO) <sup>(g)</sup>	-
$\Delta_v^p$ (band calculation)	-	-	-8.5(TB) <sup>(c)</sup> (FCC)	-8.5(TB) <sup>(c)</sup> (FCC)	4.8(APW) <sup>(d)</sup> -10(TB) <sup>(e)</sup> 6.6(LMTO) <sup>(f)</sup> -8.5(LMTO) <sup>(g)</sup>	-

TABLE V

Compound Cluster	$V_{xx}$ ( $a_0^{-3}$ )	$V_{yy}$ ( $a_0^{-3}$ )	$V_{zz}$ ( $a_0^{-3}$ )
SnO [SnO <sub>8</sub> Sn <sub>12</sub> ]	+1.97 (1.0, 0.0, 0.0)	+1.97 (0.0, 1.0, 0.0)	-3.95 (0.0, 0.0, 1.0)
SnF <sub>2</sub> [SnF <sub>11</sub> Sn <sub>4</sub> ]	+1.85 (0.70, -0.63, 0.32)	+2.09 (-0.28, -0.66, -0.69)	-3.94 (0.65, 0.40, -0.64)
SnS [SnS <sub>7</sub> Sn <sub>8</sub> ]	+1.37 (0.92, -0.40, 0.0)	+1.42 (0.0, 0.0, 1.0)	-2.79 (0.40, 0.92, 0.0)
SnSe [SnSe <sub>7</sub> Sn <sub>8</sub> ]	+1.06 (0.0, 0.0, 1.0)	+1.11 (0.93, -0.37, 0.0)	-2.17 (0.37, 0.93, 0.0)
SnO <sub>2</sub> [SnO <sub>10</sub> Sn <sub>10</sub> ]	-0.26 (0.0, 1.0, 0.0)	-0.31 (0.0, 0.0, 1.0)	+0.57 (1.0, 0.0, 0.0)
SnF <sub>2</sub> [SnF <sub>22</sub> Sn <sub>4</sub> ]	+1.17 (1.0, 0.0, 0.0)	+1.19 (0.0, 1.0, 0.0)	-2.37 (0.0, 0.0, 1.0)

TABLE VI

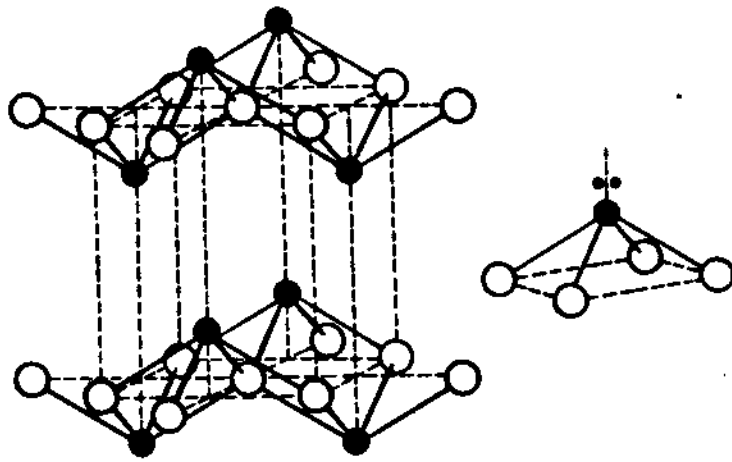
Compound	Contribution of shallow core orbitals (4s+4p+4d) ( $a_0^{-3}$ )	Contribution of Valence orbitals ( $a_0^{-3}$ )				Contribution of Valence orbitals ( $a_0^{-3}$ )				
		5p <sub>z</sub>	5p <sub>y</sub>	5p <sub>x</sub>	Other orbitals	Total	"lone pair"	Remaining orbitals	Total	
SnO	+0.423	+1.61	+1.62	-7.55	-0.031	-4.35	13a <sub>1</sub> 15a <sub>1</sub>	-1.68 -4.54	+1.87	-4.35
SnS	+0.060	-4.15	+1.84	+0.004	+0.004	-2.31	28a'	-2.43	+0.12	-2.31
SnSe	+0.041	-3.45	+1.59	+0.001	+0.001	-1.86	28a'	-2.23	+0.37	-1.86
SnO <sub>2</sub>	-0.057	-3.74	+2.20	+2.29	-0.081	+0.67			-	
SnF <sub>4</sub>	-0.034	+1.71	+1.71	-5.85	-0.007	-2.44			-	



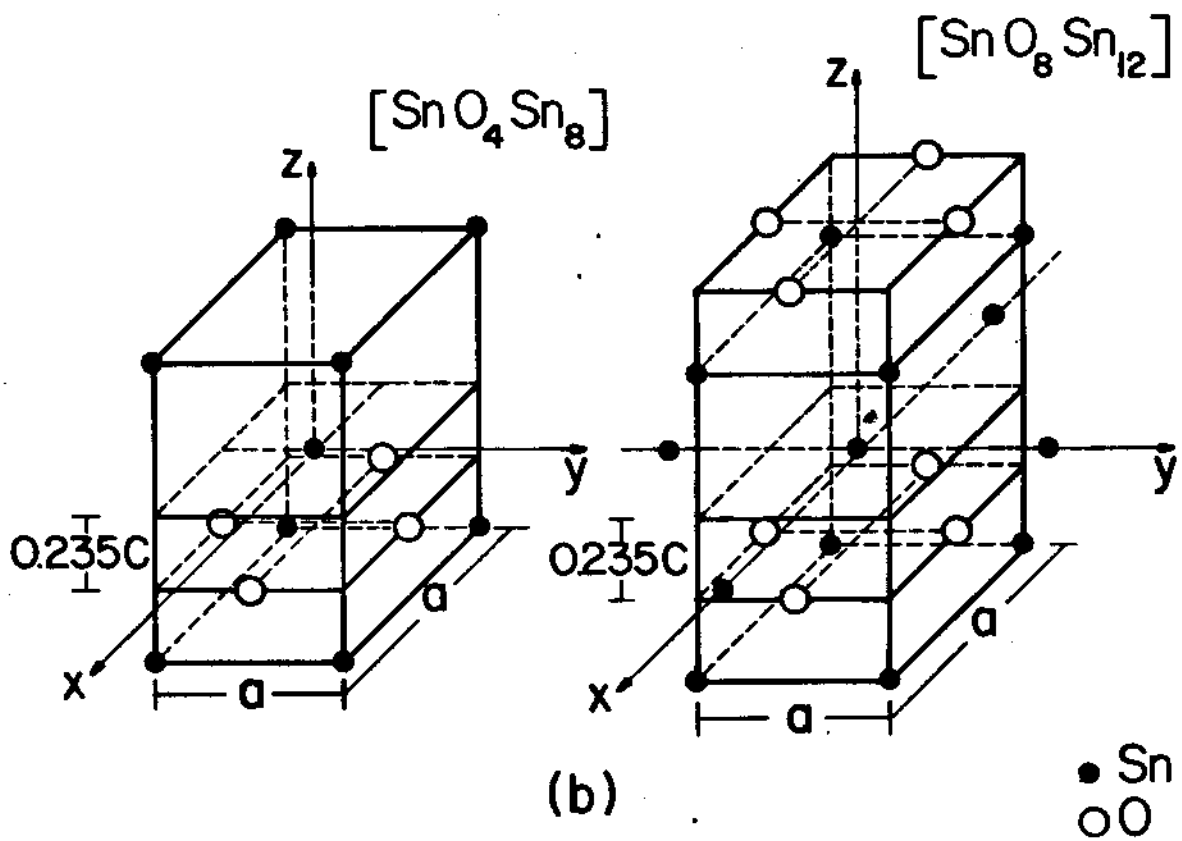
TABLE VII

Compound	Cluster	$V_{zz}$ ( $a_0^{-3}$ )	$\eta$	$\Delta EQ$ (mm/s) calculated	$ \Delta EQ $ (mm/s) experimental
SnO	[SnO <sub>8</sub> Sn <sub>12</sub> ]	-3.95	0.0	+2.62	1.45 <sup>(a)</sup>
SnF <sub>2</sub>	[SnF <sub>11</sub> Sn <sub>4</sub> ]	-3.94	0.059	+2.62	2.20 <sup>(a)</sup>
SnS	[SnS <sub>7</sub> Sn <sub>8</sub> ]	-2.79	0.018	+1.85	0.86 <sup>(d)</sup>
SnSe	[SnSe <sub>7</sub> Sn <sub>8</sub> ]	-2.17	0.021	+1.44	0.75 <sup>(b)</sup>
SnO <sub>2</sub>	[SnO <sub>10</sub> Sn <sub>10</sub> ]	+0.57	0.091	-0.379	0.45 <sup>(c)</sup>
SnF <sub>4</sub>	[SnF <sub>22</sub> Sn <sub>4</sub> ]	-2.37	0.0	+1.57	1.66 <sup>(a)</sup>

## SnO

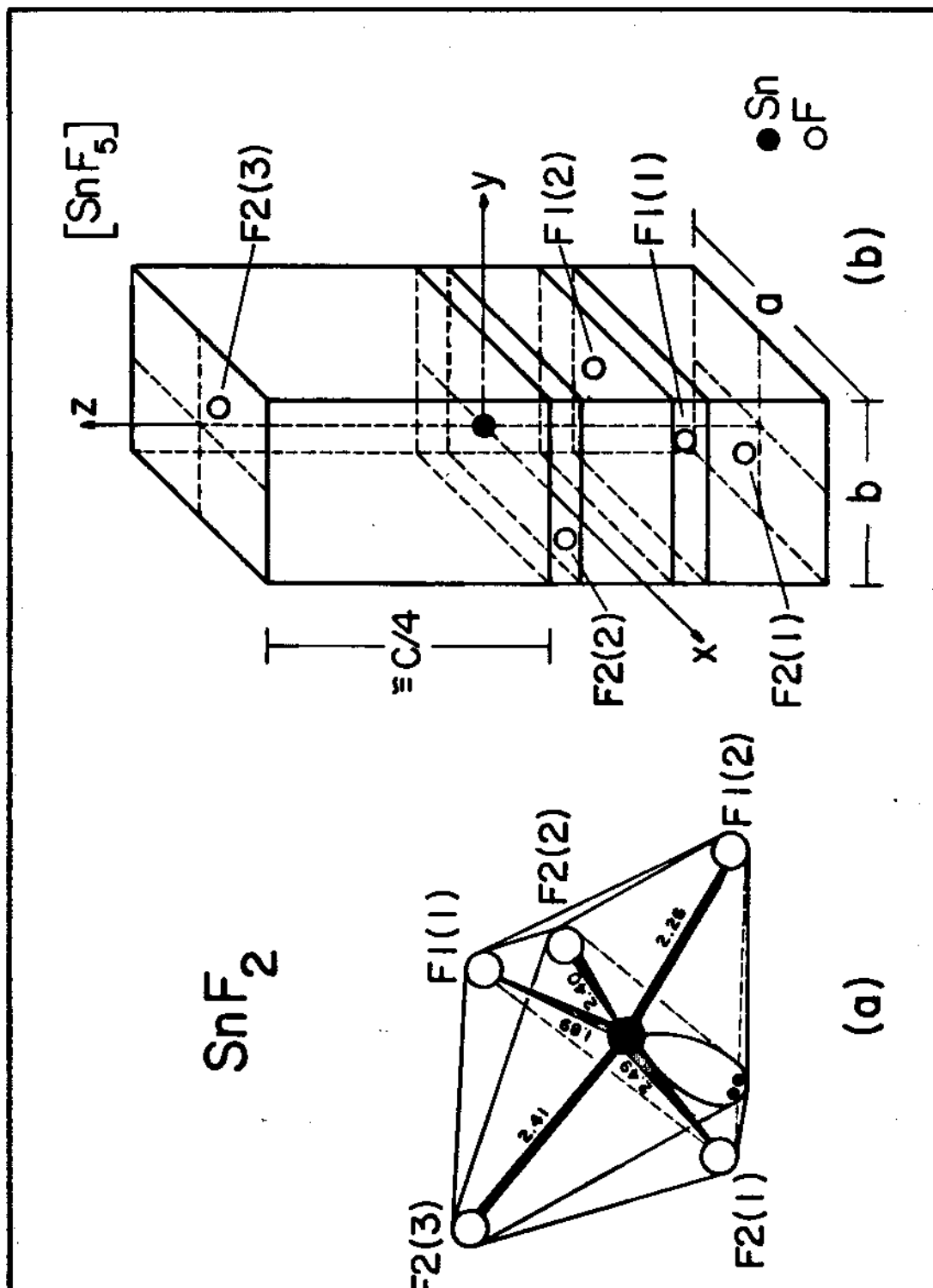


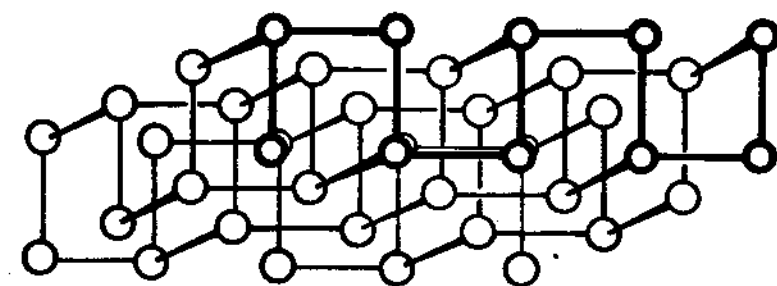
(a)



(b)

Fig. 1





(a)

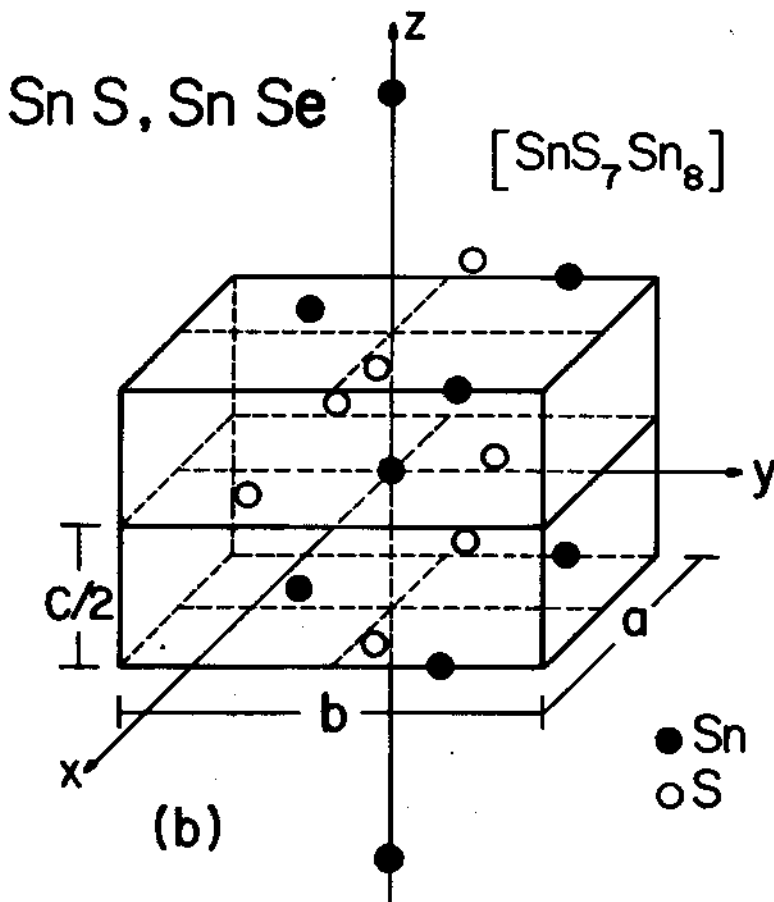


Fig. 3

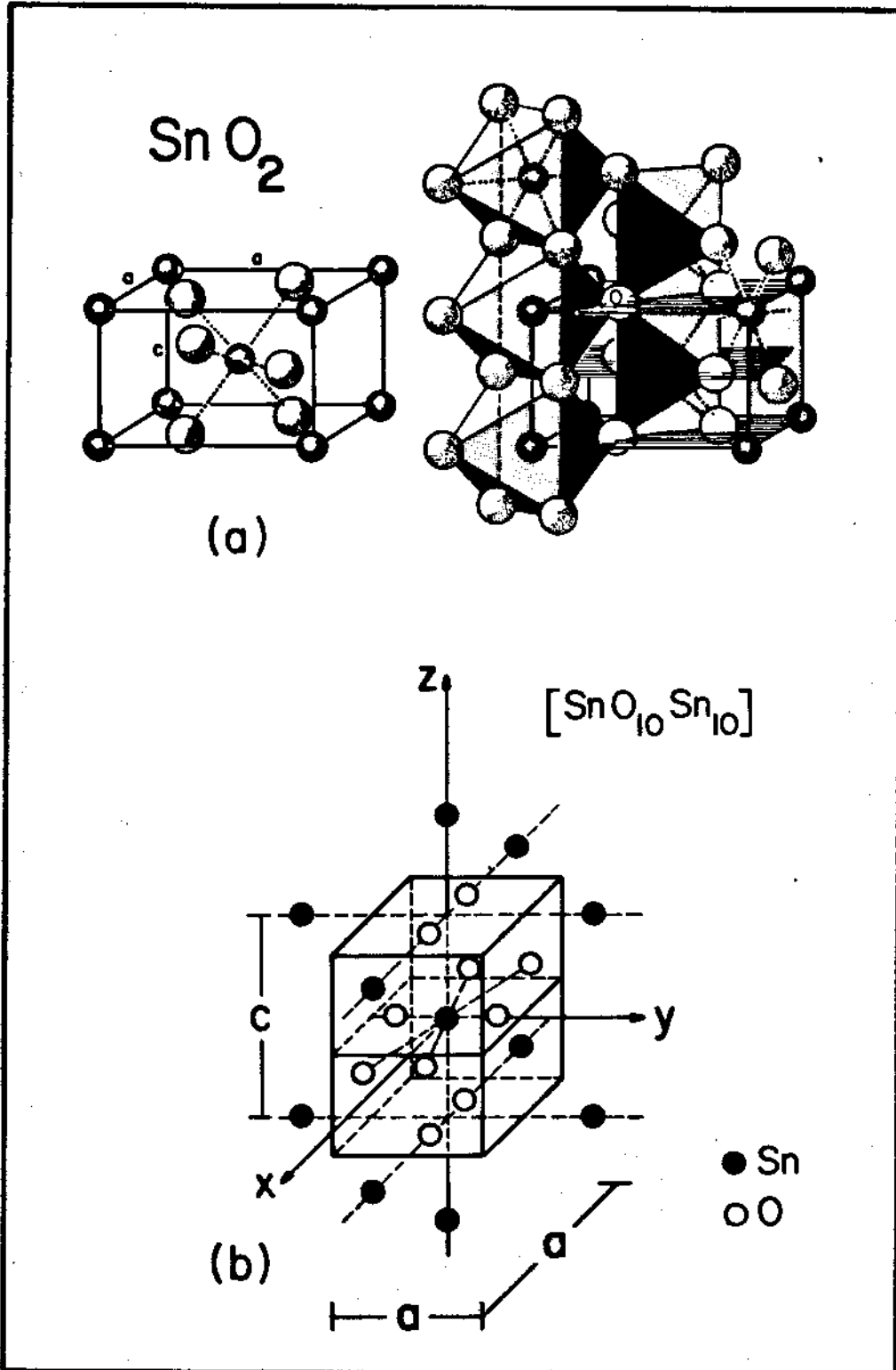
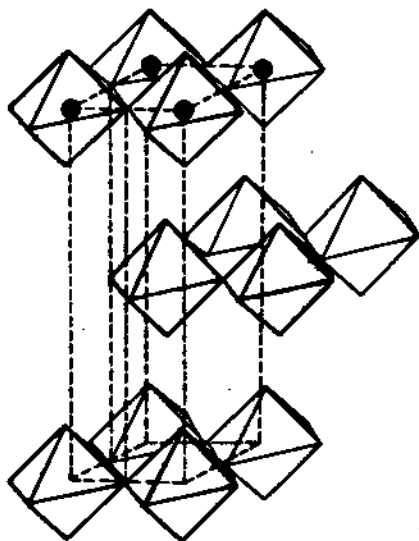
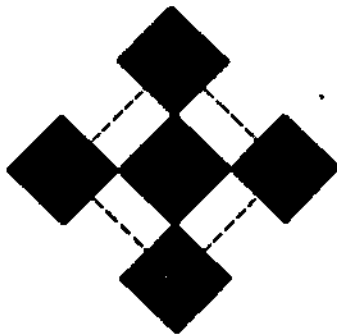


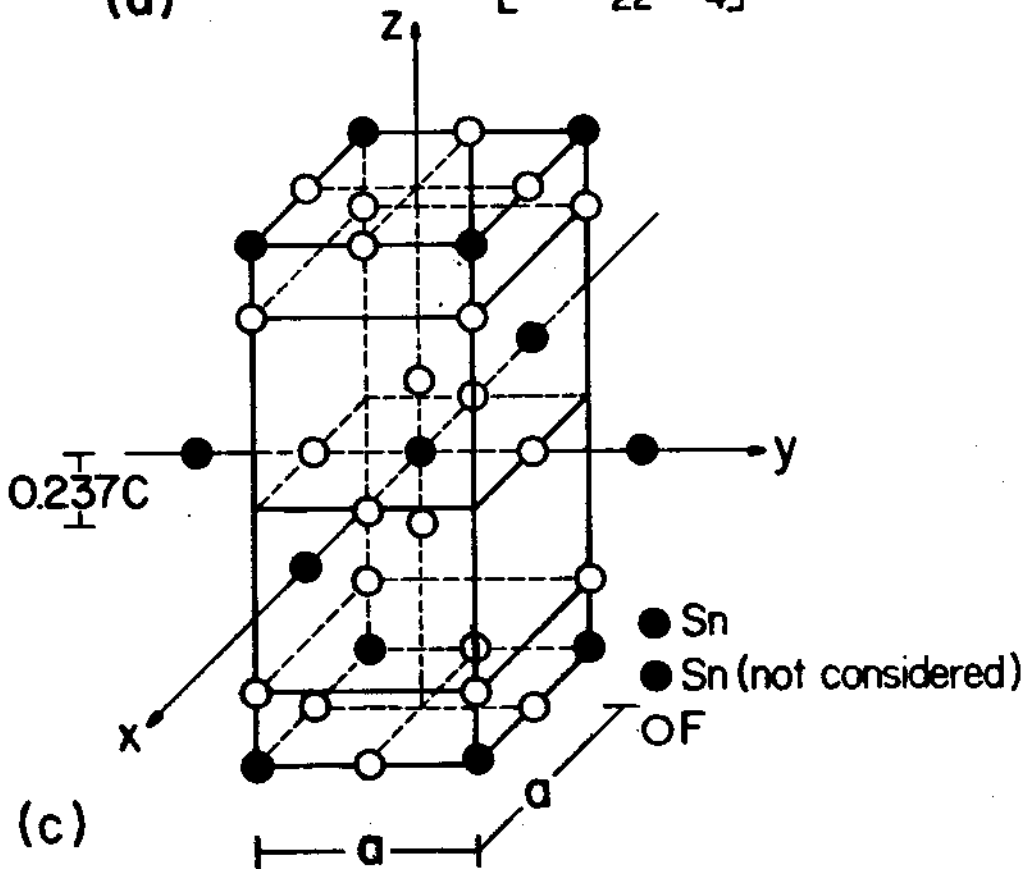
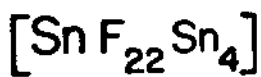
Fig. 4



(a)



(b)



(c)

Fig. 5

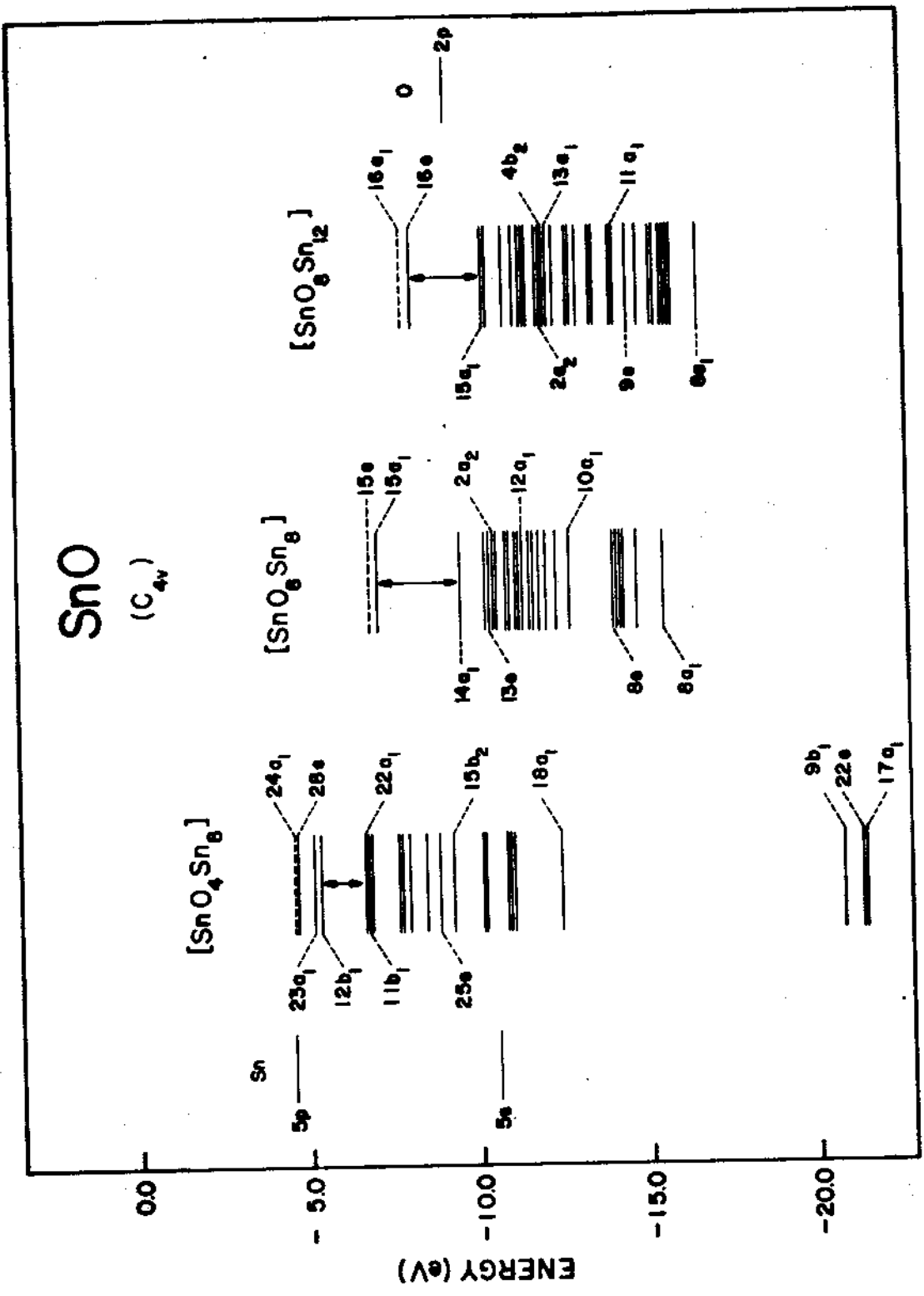


Fig. 6

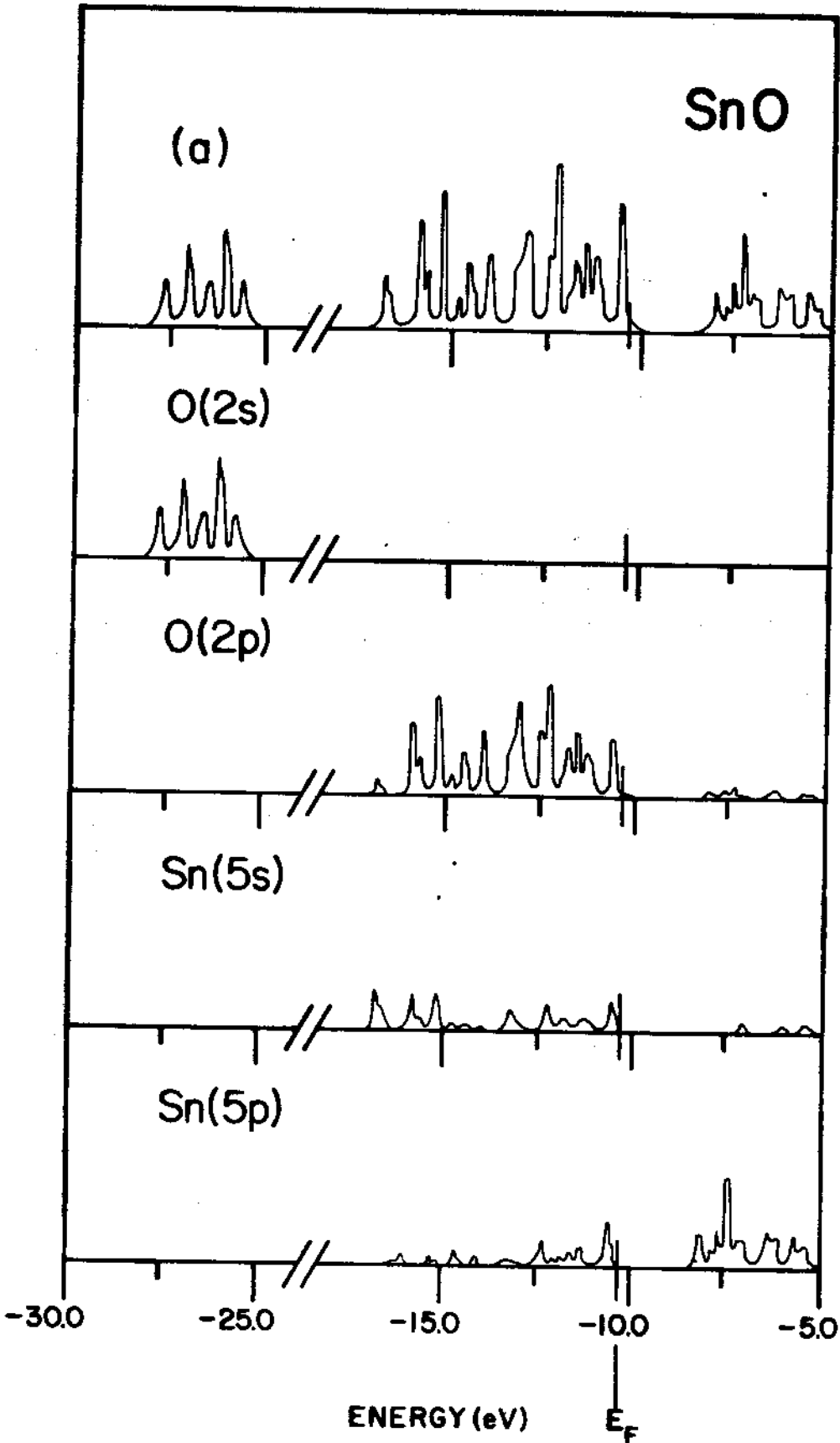


Fig. 7



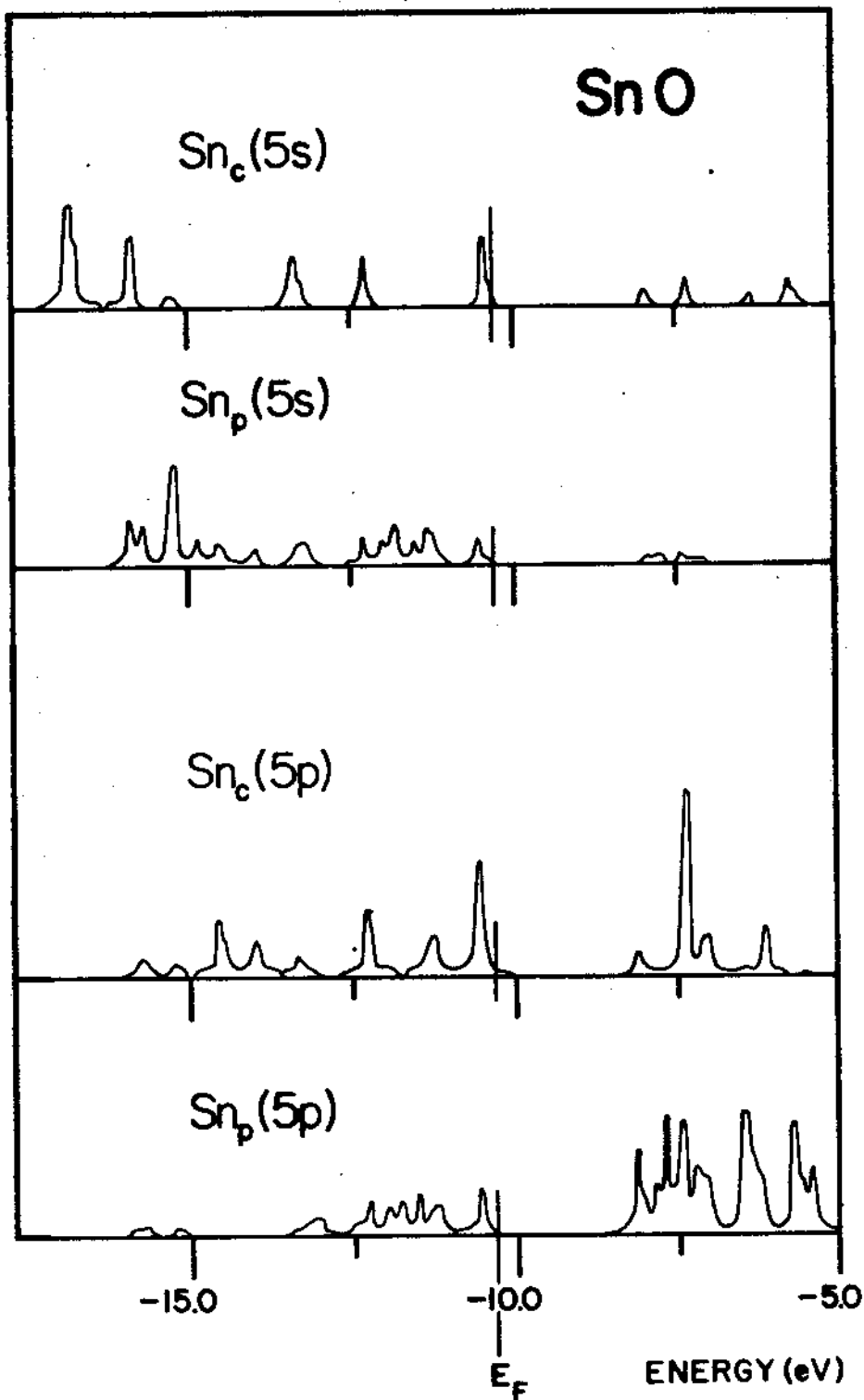


Fig. 8

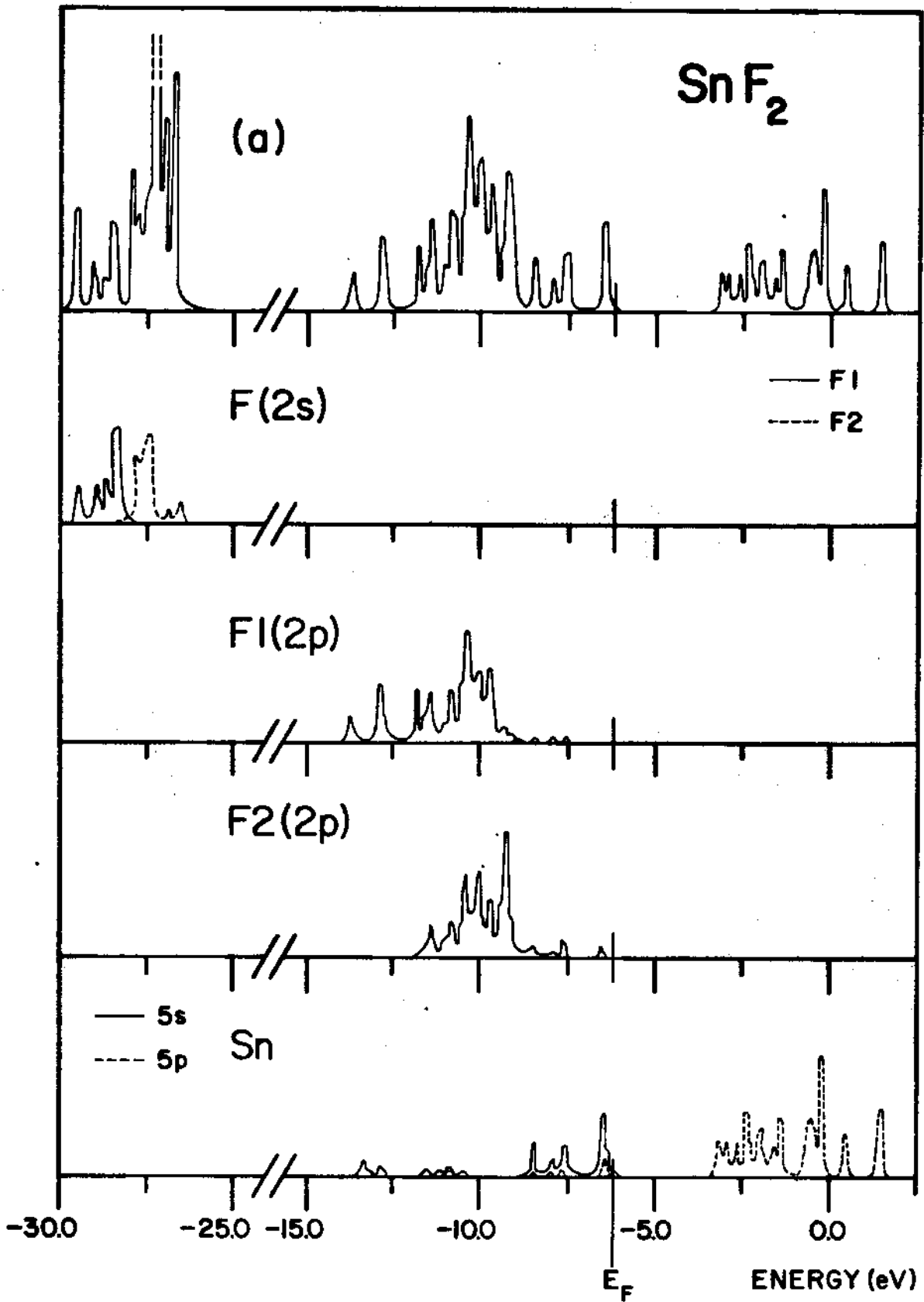


Fig. 9

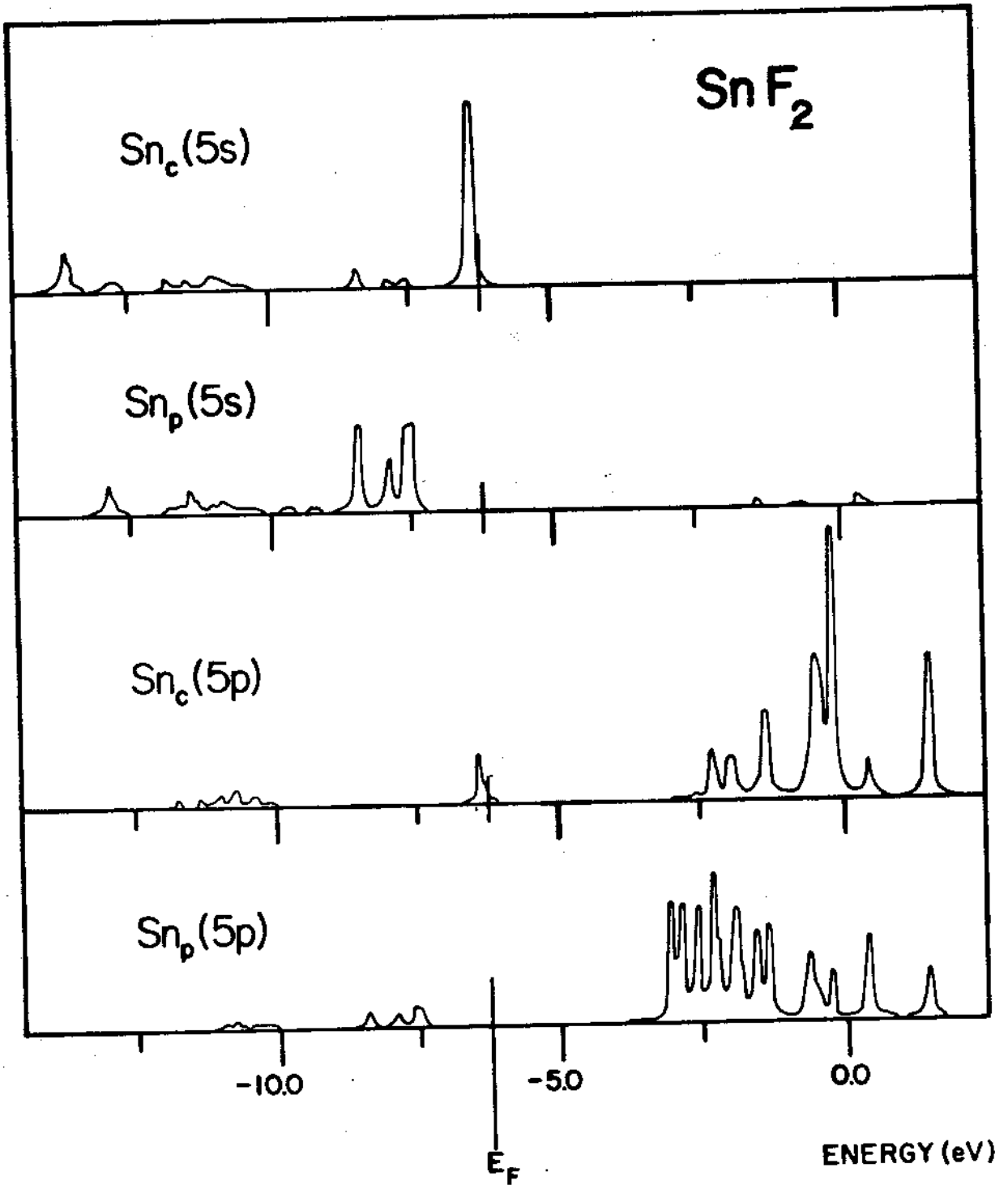


Fig. 10

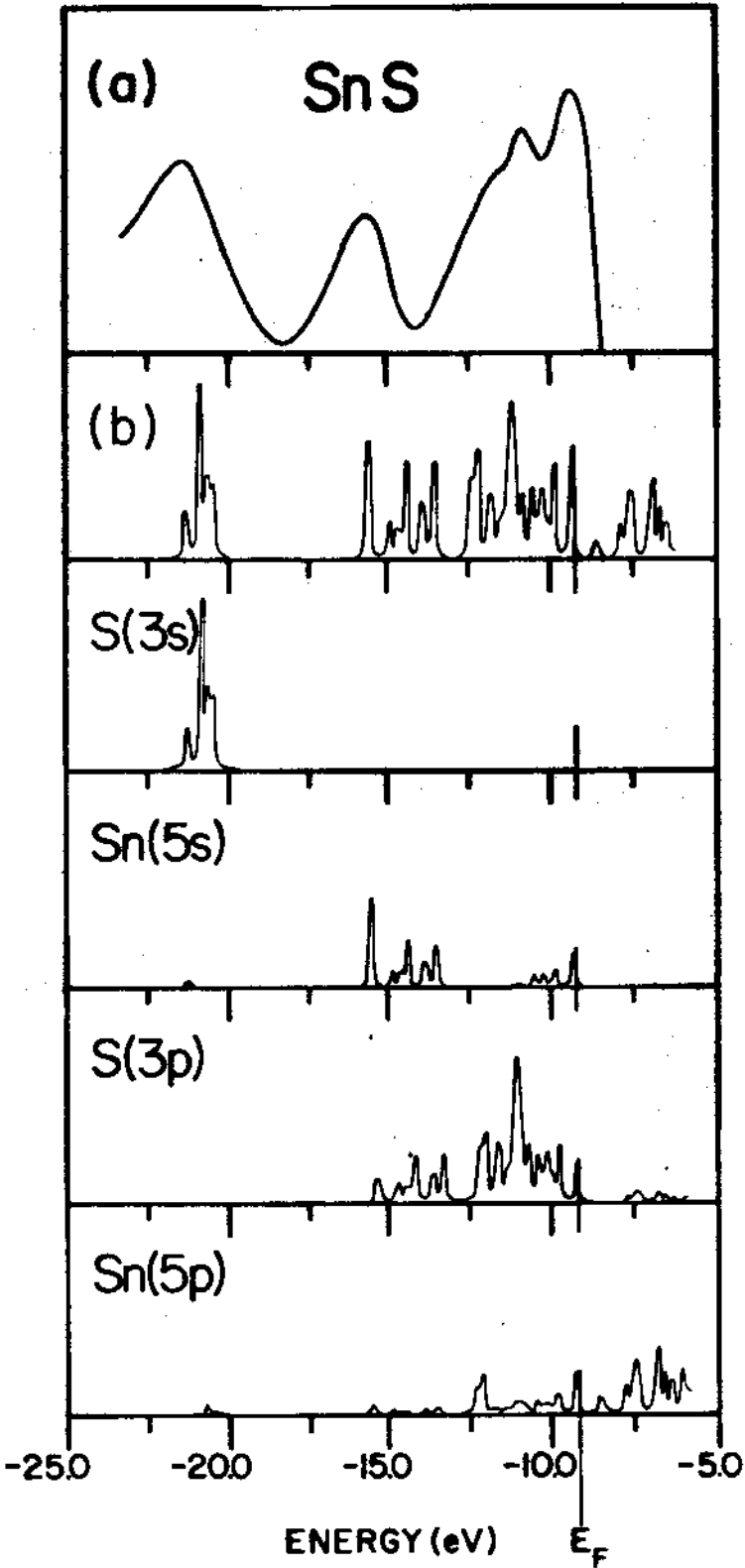


Fig. 11

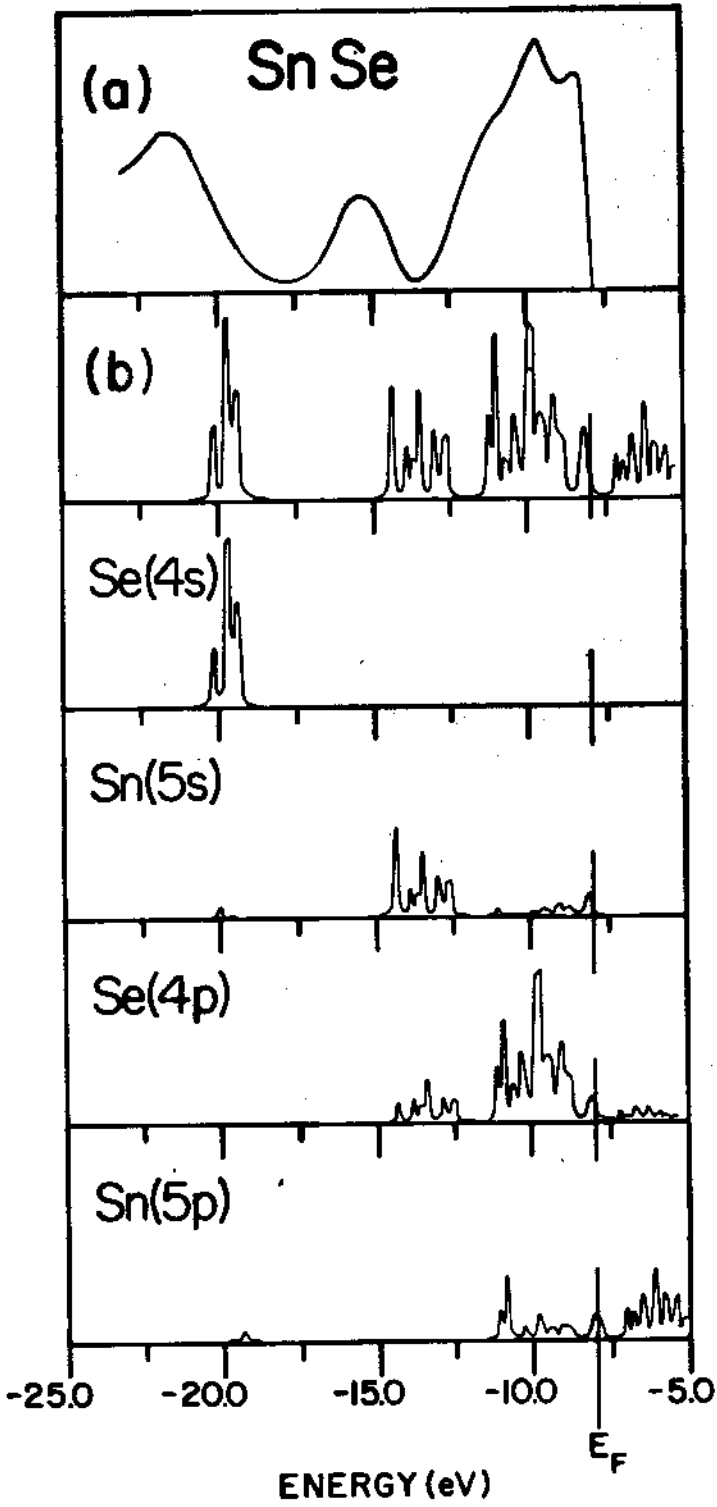


Fig. 12

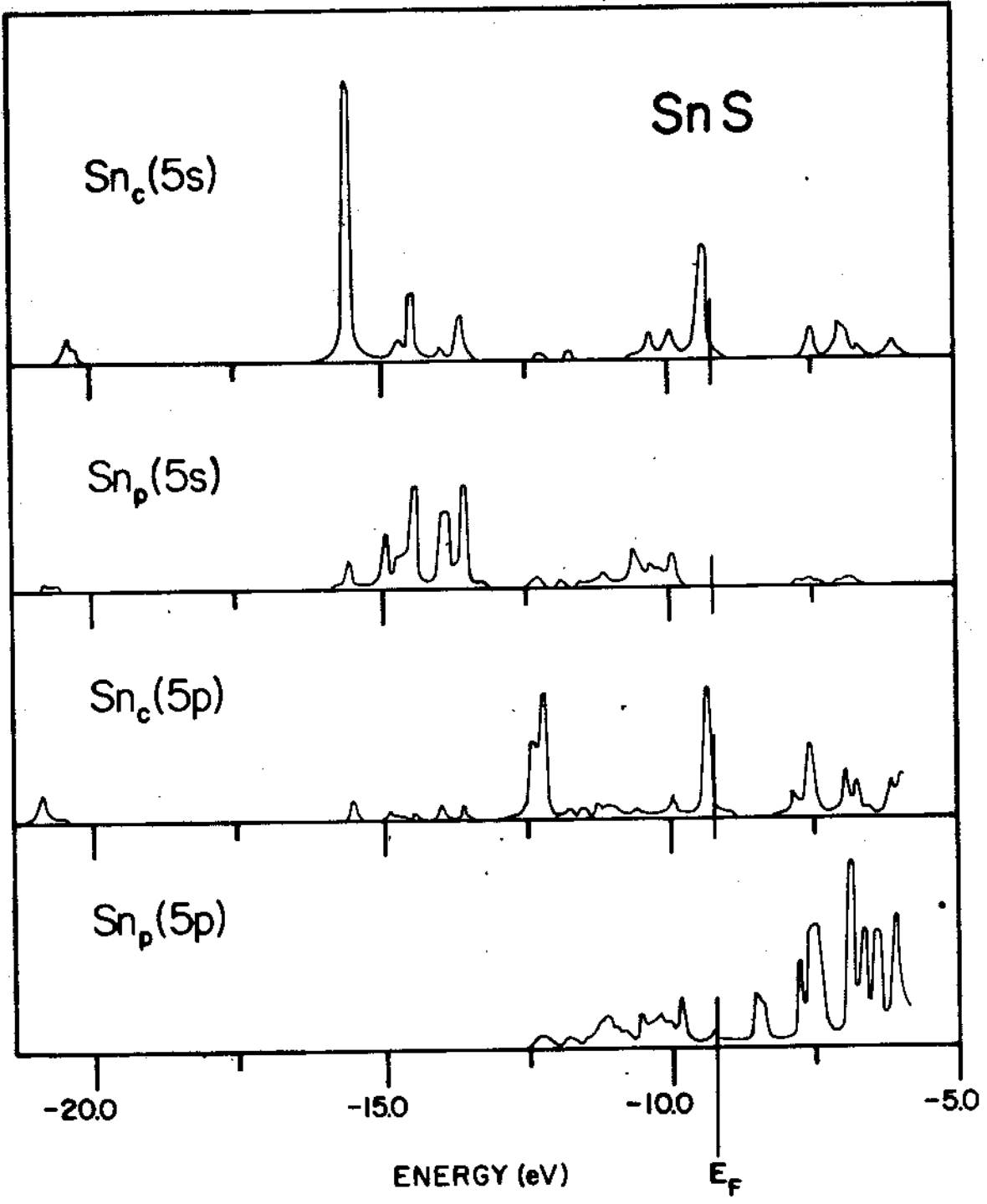


Fig. 13

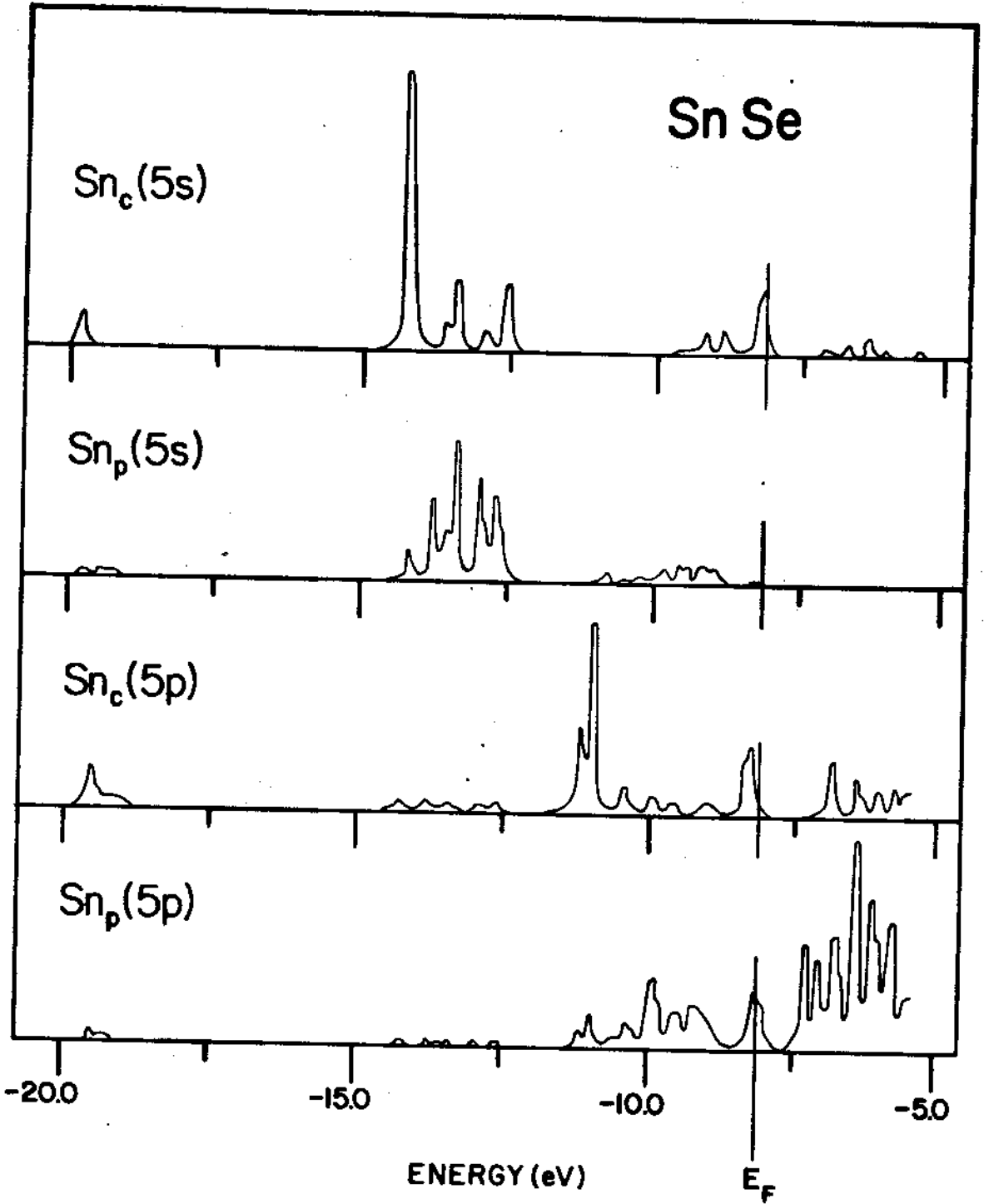


Fig. 14

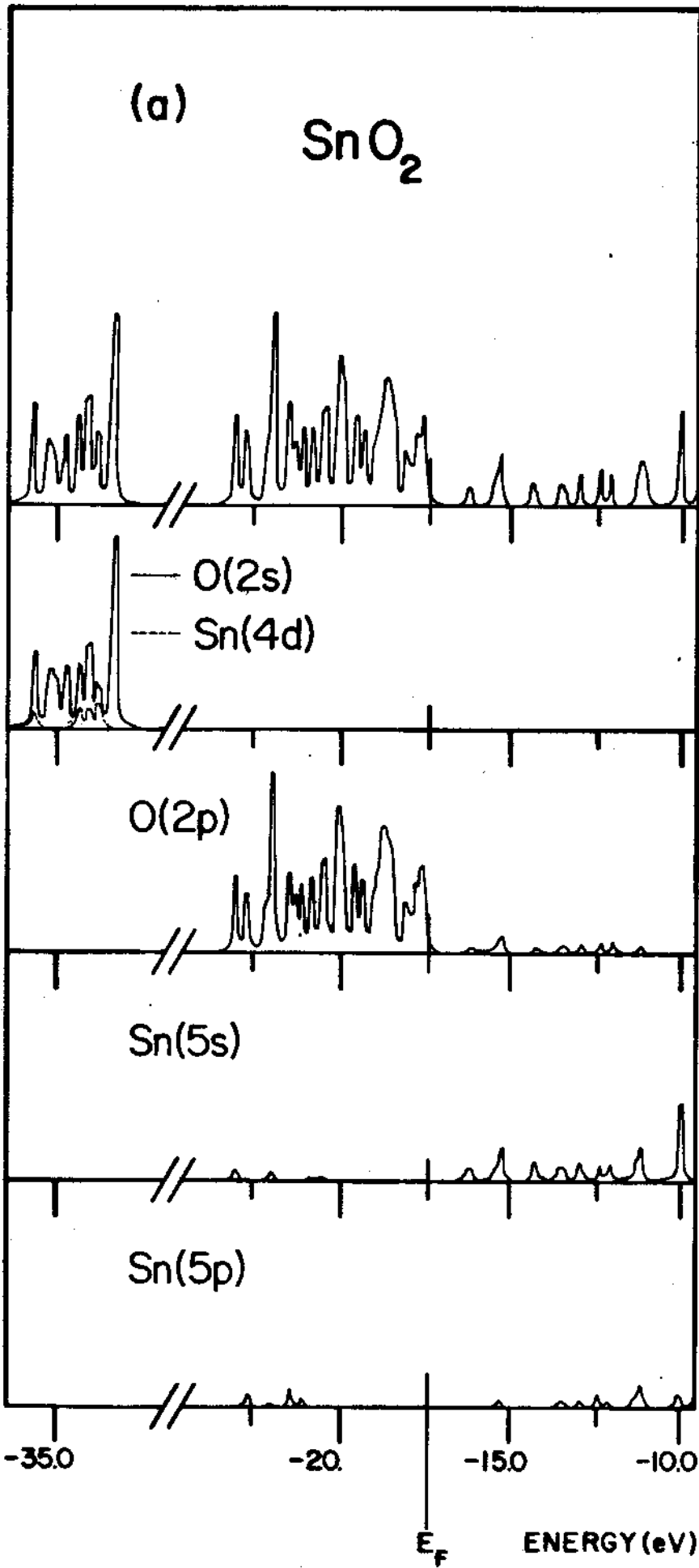


Fig. 15



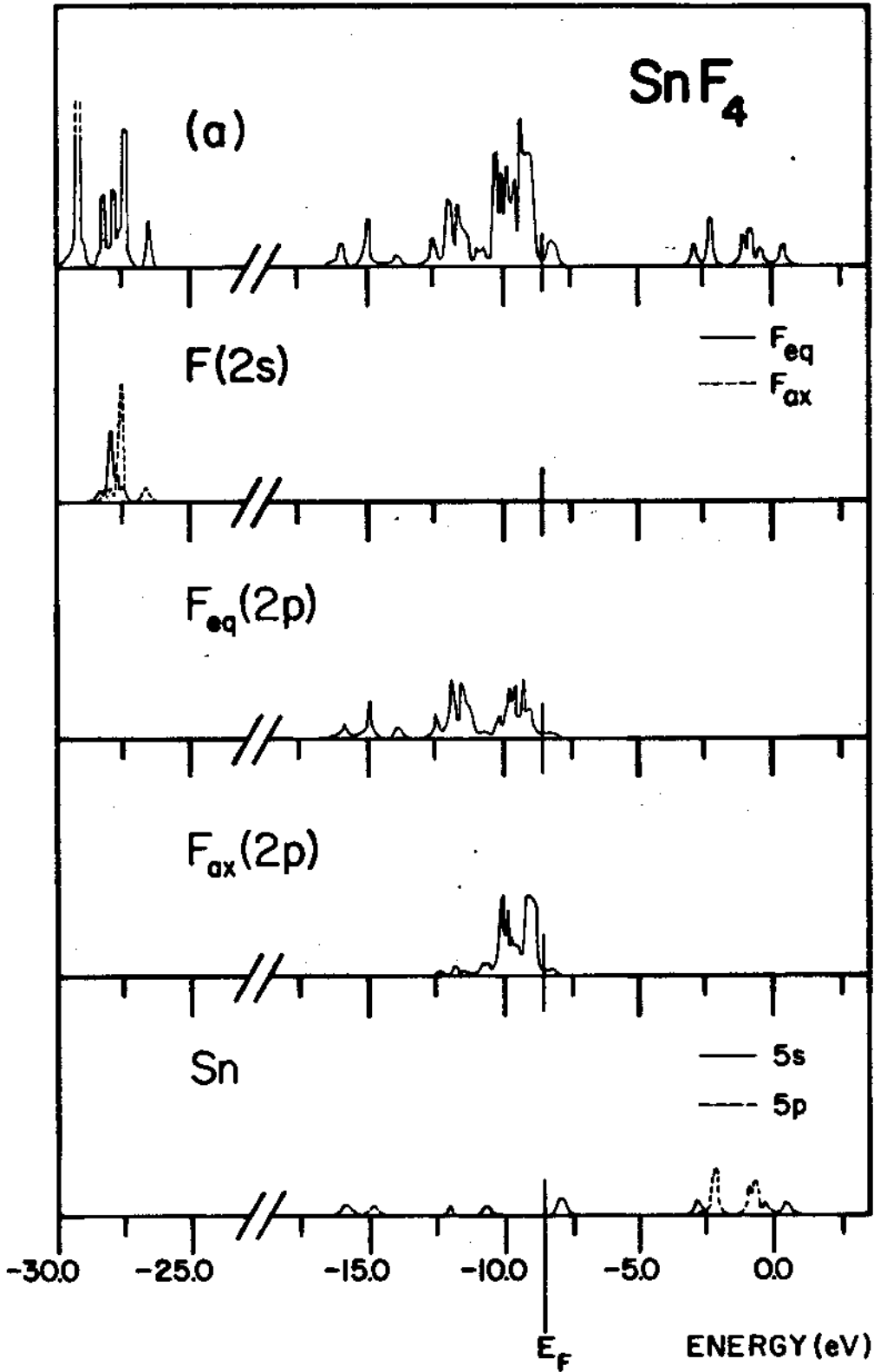


Fig. 16

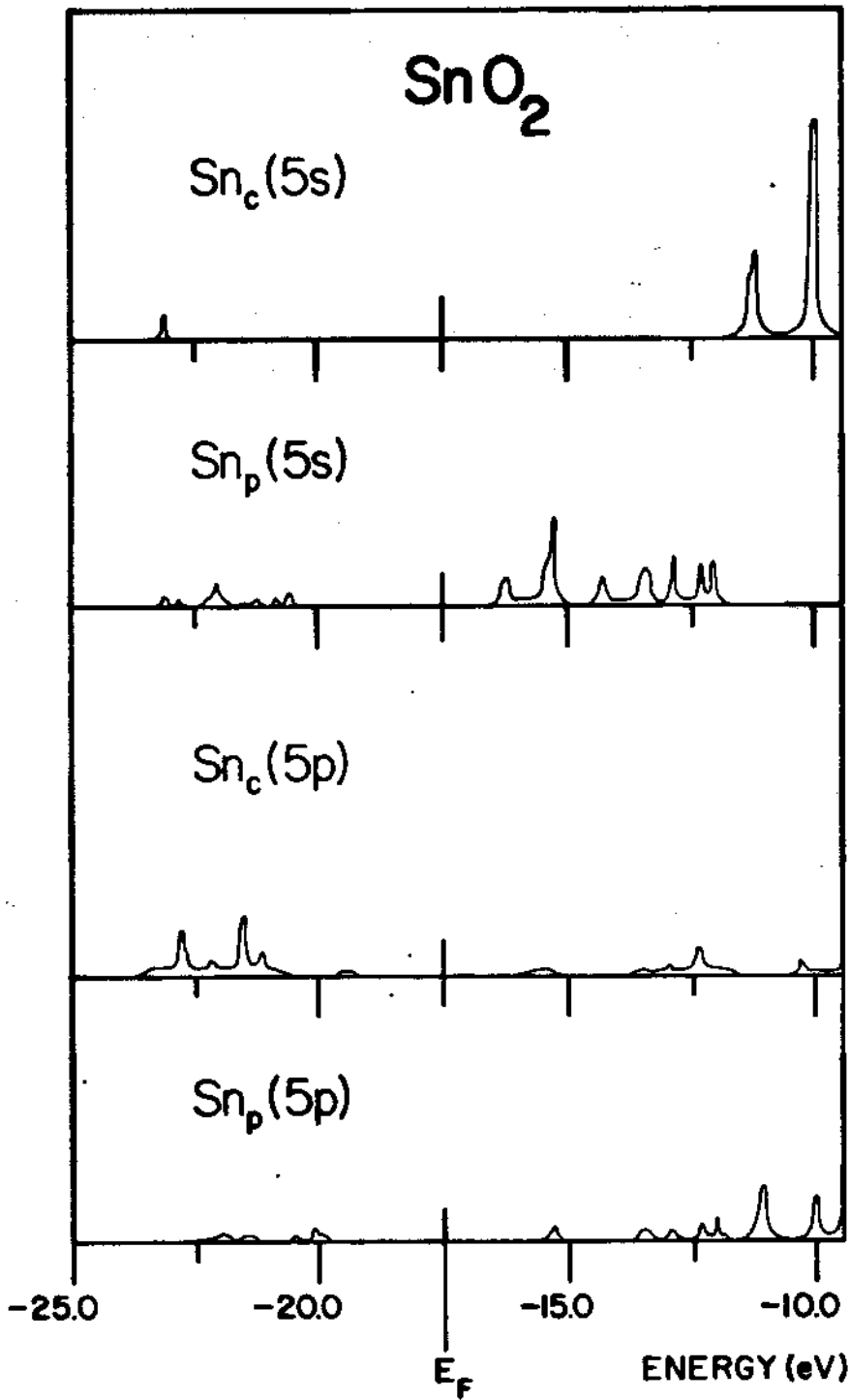


Fig. 17

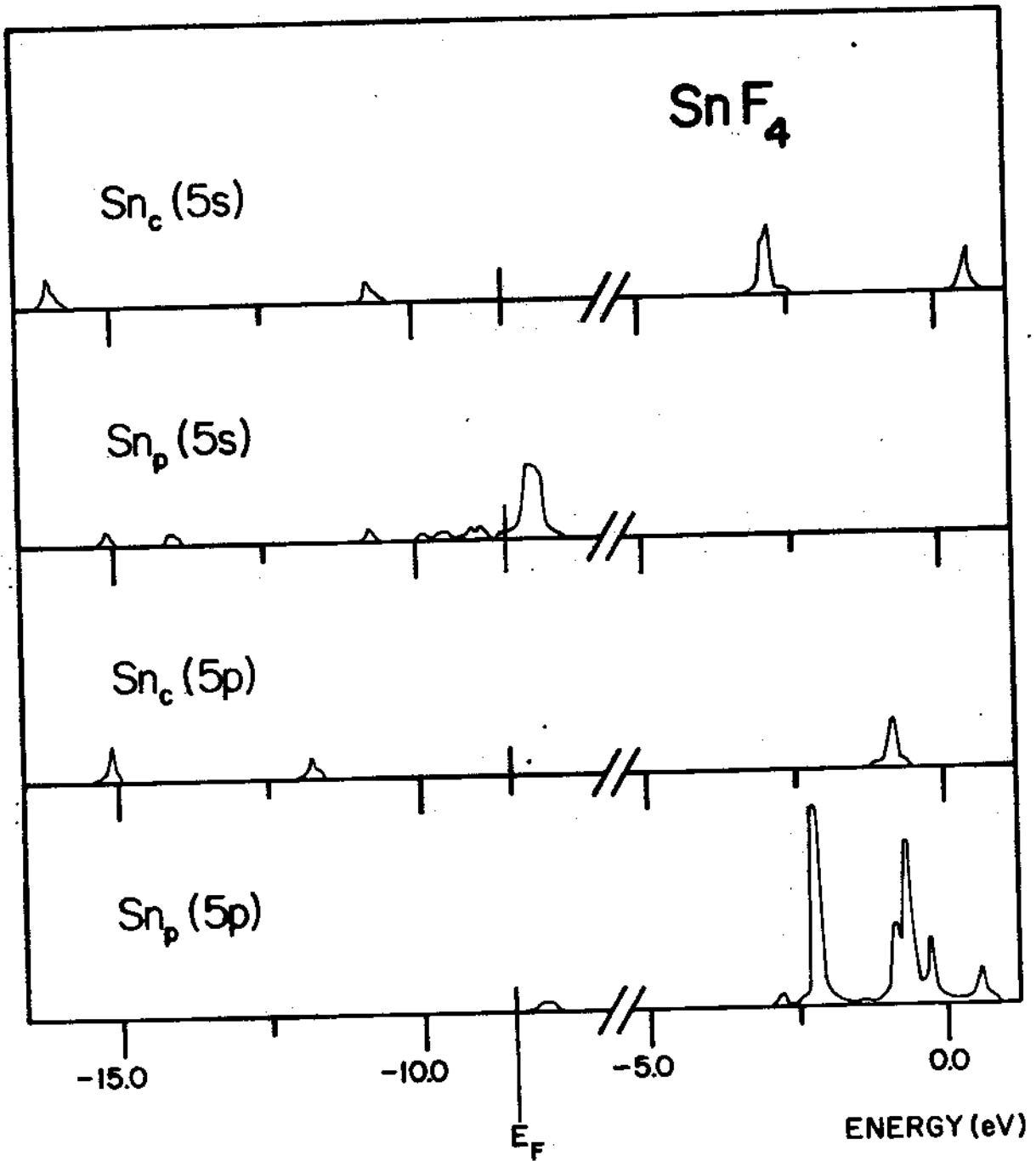


Fig. 18

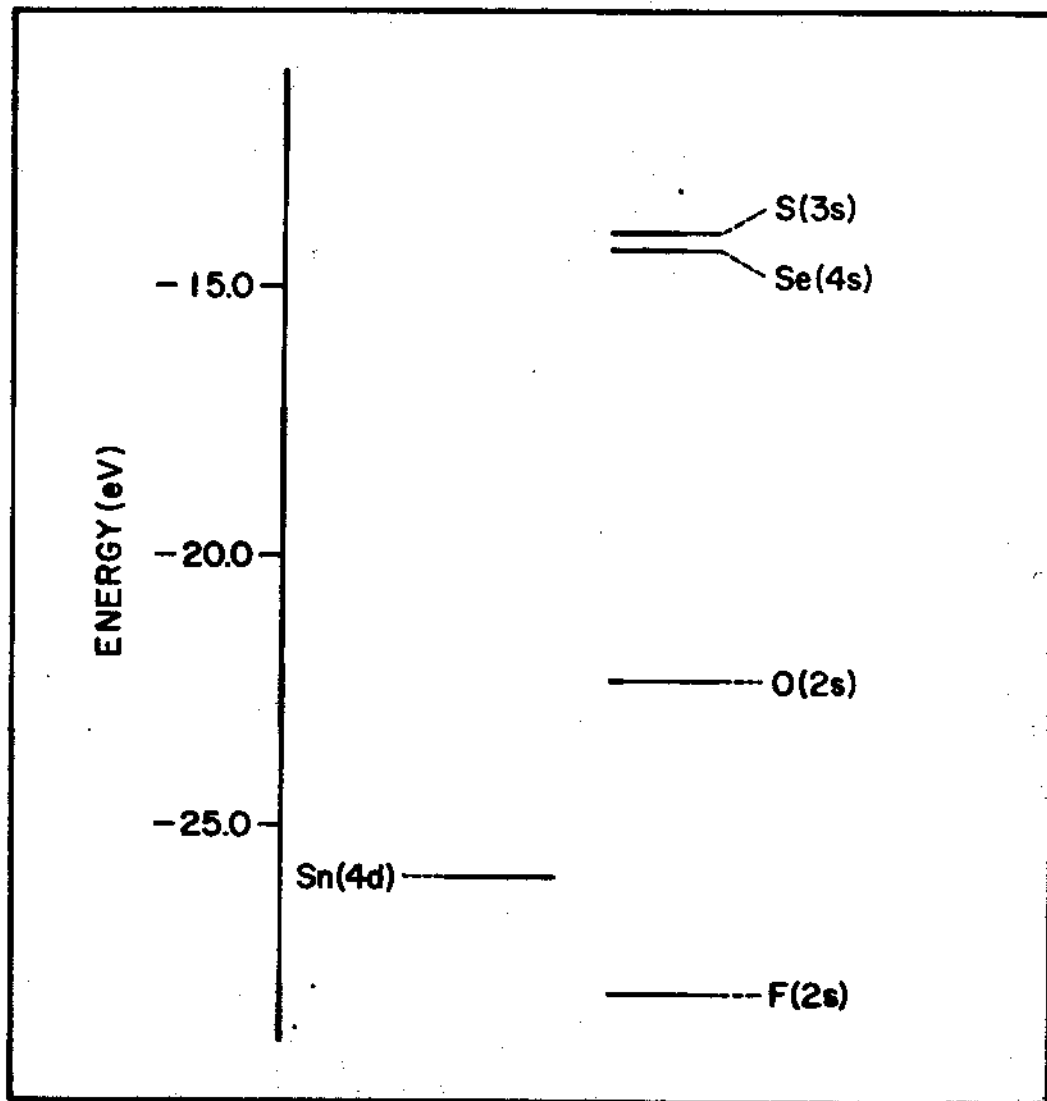


Fig. 19

## REFERENCES

- 1) P. Blaha, K. Schwarz and P. Herzig, Phys. Rev. Letters 54, 1192 (1985).
- 2) D. Guenzburger and D.E. Ellis, Phys. Rev. B36, 6971 (1987); D. Guenzburger and D.E. Ellis, Hyperfine Interac. 60, 635 (1990).
- 3) N.N. Greenwood and T.C. Gibb, "Mössbauer Spectroscopy", Chapman and Hall, London (1971).
- 4) Landolt - Börnstein, vol. 17: "Semiconductors", eds. O. Madelung, M. Schulz and H. Weiss, Springer-Verlag, Berlin (1983).
- 5) D.E. Ellis and G.S. Painter, Phys. Rev. B2, 2887 (1970); D.E. Ellis, Int. J. Quant. Chem. S2, 35 (1968).
- 6) P. Hohenberg and W. Kohn, Phys. Rev. B136, 864 (1964); J. Callaway and N.H. March, "Density Functional Methods: Theory and Applications" in "Solid State Physics", vol. 38, Academic Press, N. York (1984).
- 7) W. Kohn and L.J. Sham, Phys. Rev. A140, 1133 (1965).
- 8) L. Hedin and B.I. Lundqvist, J. Phys. C4, 2064 (1971).
- 9) A.H. Stroud, "Approximate Calculation of Multiple Integrals", Prentice Hall, Englewood Cliffs, N.J. (1971).
- 10) B. Delley and D.E. Ellis, J. Chem. Phys. 76, 1949 (1982).
- 11) D.E. Ellis, G.A. Benesh and E. Byrom, Phys. Rev. B16, 3308 (1977).
- 12) J.C. Slater, "Insulators, Semiconductors and Metals", McGraw-Hill, N. York (1967), pg. 215.
- 13) R.S. Mulliken, J. Chem. Phys. 46, 497 (1949).
- 14) P.-L. Cao, D.E. Ellis and A.J. Freeman, Phys. Rev. B 25, 2124 (1982).
- 15) A.F. Wells, "Structural Inorganic Chemistry", 5<sup>th</sup> edition, Clarendon Press, Oxford (1984).
- 16) J. Pannetier and G. Denes, Acta Cryst. B36, 2763 (1980).
- 17) G. Denes, J. Pannetier and J. Lucas, J. Solid State Chem., 33, 1 (1980).
- 18) R.W.G. Wyckoff, "Crystal Structures", vol. 1, J. Wiley & Sons, N. York (1964).
- 19) F.D. Bloss, "Crystallography and Crystal Chemistry", Holt, Rinehart and Winston, N. York (1971); J.O. Dimmock and R.G. Wheeler, Phys. Rev. 127, 391, (1962).

- 20) R.W.G. Wyckoff, "Crystal Structures", vol. 2, J. Wiley & Sons, N. York (1964).
- 21) J.C. Slater, "The Self-Consistent-Field for Molecules and Solids", "Quantum Theory of Molecules and Solids", vol. 4, McGraw-Hill, N. York (1974).
- 22) P.C. Kemeny, J. Azoulay, M. Cardona and L. Ley, Nuovo Cimento 39, 709 (1977).
- 23) A.P. Lambros, D. Geraleas and N.A. Economou, J. Phys. Chem. Solids, 35, 537 (1974).
- 24) A.M. Elkorashy, J. Phys. Chem. Solids, 50, 893 (1989).
- 25) P.L. Gobby and G.J. Lapeyre, in "Proc. of the 13<sup>th</sup> Int. Conf. on Semiconductors", ed. F. Fumi, Rome (1976) (cited in Refs. (28) and (29)).
- 26) J. Robertson, Phys. Rev. B28, 4671 (1983).
- 27) F.J. Arlinghaus, J. Phys. Chem. Solids 35, 931 (1974).
- 28) J. Robertson, J. Phys. C12, 4767 (1979).
- 29) A. Svane and E. Antoncik, J. Phys. Chem. Solids 48, 171 (1987).
- 30) N.I. Medvedeva, V.P. Zhukov, M.Ya. Khodos and V.A. Goubanov, Phys. Stat. Solidi (b) 160, 517 (1990).
- 31) A.W. Parke and G.P. Srivastava, Phys. Stat. Solidi (b) 101, K31 (1980).
- 32) R. Car, G. Gucci and L. Quartapelle, Phys. Stat. Solidi (b) 86, 471 (1978).
- 33) J.L. Jacquemin and G. Bordure, J. Phys. Chem. Solids, 36, 1081 (1975).
- 34) E.M. Baggio and T. Sonnino, J. Chem. Phys. 52, 3786 (1970).
- 35) "Chemical Applications of Mössbauer Spectroscopy", ed. V.I. Goldanskii and R.H. Herber, Academic Press, N. York (1968).
- 36) J.K. Lees and P.A. Flinn, J. Chem. Phys. 48, 882 (1968).
- 37) H. Haas, M. Menninger, H. Andreasen, S. Damgaard, H. Grann, F.T. Pedersen, J.W. Petersen and G. Weyer, Hyperfine Interac. 15/16, 215 (1983).
- 38) J. Terra and D. Guenzburger, to be published.
- 39) J. Terra and D. Guenzburger, Hyperfine Interac., 60, 627 (1990) (Proceed. VII Int. Conference on Hyperf. Interac.).